Applied Catalysis B: Environmental 249 (2019) 292–305

Contents lists available at ScienceDirect

Applied Catalysis B: Environmental

journal homepage: www.elsevier.com/locate/apcatb

The role of defect sites and oxophilicity of the support on the phenol hydrodeoxygenation reaction

Camila A. Teles[a,b], Priscilla M. de Souza[a,1], Adriano Henrique Braga[c], Raimundo C. Rabelo-Neto[a], Alejandra Teran[d], Gary Jacobs[d,e], Daniel E. Resasco[f], Fabio B. Noronha[a,b,*]

[a] Catalysis Division, National Institute of Technology, Av. Venezuela 82, 20081-312, Rio de Janeiro, RJ, 20081-312, Brazil
[b] Military Institute of Engineering, Chemical Engineering Department, Praça Gal. Tiburcio 80, Rio de Janeiro, 22290-270, Brazil
[c] University of São Paulo - USP, Institute of Chemistry, Av. Prof. Lineu Prestes 748, São Paulo, 05508-000, Brazil
[d] University of Texas at San Antonio, Chemical Engineering Program, Department of Biomedical Engineering, 1 UTSA Circle, San Antonio, TX, 78249 USA
[e] University of Texas at San Antonio, Department of Mechanical Engineering, 1 UTSA Circle, San Antonio, TX, 78249 USA
[f] Center for Biomass Refining, School of Chemical, Biological, and Materials Engineering, The University of Oklahoma, Norman, OK, 73019, USA

ARTICLE INFO

Keywords:
Phenol
Hydrodeoxygenation
Bio-oil
Stability
Oxygen vacancy
Defect sites

ABSTRACT

This work studies the effect of support defect sites on the performance of $Pd/Ce_xZr_{1-x}O_2$ (x = 0.00; 0.25; 0.50; 0.75; 0.90) catalysts for the hydrodeoxygenation of phenol in the gas phase at 573 K. The activity and selectivity for hydrodeoxygenation of phenol depends significantly on the support used. Increasing the Zr content from x = 0.0 to 0.5, the reaction rate for hydrodeoxygenation and the selectivity to benzene remains very low. However, upon increasing the Zr content above x = 0.5 a sudden jump in reaction rate and selectivity to benzene is observed. Interestingly, this activity and selectivity boost has no direct correlation with the density of acid sites or the concentration of defects on the support. Rather, the selectivity to deoxygenated products is found to depend on the oxophilicity of the support. Increasing the Zr content enhances the strength of the interaction between the O of the carbonyl group and the oxophilic site. It is proposed that the oxophilicity of these catalysts is related to the structure of the $Ce_xZr_{1-x}O_2$ solid solution formed. In addition, it is observed that the degree of deactivation during the reaction also depends on the Ce/Zr molar ratio of the support. Pd/ZrO_2, $Pd/Ce_{0.10}Zr_{0.90}O_2$ and $Pd/Ce_{0.25}Zr_{0.75}O_2$ catalysts readily deactivate during reaction, whereas the phenol conversion only slightly decreases for Pd/CeO_2, $Pd/Ce_{0.75}Zr_{0.25}O_2$ and $Pd/Ce_{0.50}Zr_{0.50}O_2$ catalysts. The results reveal that the density of Zr species on the surface is responsible for catalyst deactivation. The stronger adsorption between the oxygen from the phenol with Zr cations resulted in an accumulation of O-containing byproducts and catalyst deactivation.

1. Introduction

Bio-oil obtained from fast pyrolysis of lignocellulosic biomass contains high amounts of oxygen-containing compounds and must be upgraded to improve its stability and energy density. The upgrading can be accomplished by the hydrodeoxygenation (HDO) process. However, the chemical composition of bio-oil is very complex and thus, model molecules such as phenol have been studied to assess catalytic activity trends among different catalysts [1,2].

Different reaction pathways have been suggested for HDO of phenol: (i) hydrogenation; (ii) direct deoxygenation and (iii) tautomerization. In route (i), phenol hydrogenation to cyclohexanol occurs followed by its dehydration [3,4]. This route is promoted by catalysts with sufficiently acidic supports. Route (ii) involves the hydrogenolysis of the $C(sp^2)-O$ bond. Recently, it has been suggested that more oxophilic metals such as Ru as well as supports like TiO_2 strongly interact with the oxygen atom, reducing the energy barrier to break this bond, leading to the formation of hydrogenolysis products [5–7]. Route (iii) has been recently proposed in the literature and concerns the tautomerization of phenol to the keto intermediate, 2,4-cyclohexadienone [5,8–13]. This tautomer can be hydrogenated to cyclohexanone and then cyclohexanol or produce an unsaturated alcohol (2,4-cyclohexanodiol), via C=O bond hydrogenation. The resulting alcohol is rapidly converted to benzene via dehydration. According to this reaction pathway, oxophilic supports such as TiO_2, Nb_2O_5, and ZrO_2 promote C=O hydrogenation leading to deoxygenated products.

Therefore, the support plays a key role in the HDO of phenol, opening up a selective reaction pathway. For instance, the role of

* Corresponding author.
E-mail address: fabio.bellot@int.gov.br (F.B. Noronha).
[1] Present address - Federal University of Rio de Janeiro, Chemical Engineering Program – COPPE, Rio de Janeiro, 21941-972, Brazil.

https://doi.org/10.1016/j.apcatb.2019.02.077
Received 16 October 2018; Received in revised form 6 February 2019; Accepted 28 February 2019
Available online 01 March 2019
0926-3373/

different supports (SiO_2, Al_2O_3, ZrO_2, TiO_2, Nb_2O_5, CeO_2 and $Ce_{0.5}Zr_{0.5}O_2$) on the HDO of phenol was previously investigated [9,14–16]. Supports such as SiO_2, Al_2O_3, CeO_2 and $CeZrO_2$ favored hydrogenation of the C=C ring, producing cyclohexanone and cyclohexanol. On the other hand, supports containing oxophilic sites such as ZrO_2, TiO_2 and Nb_2O_5 promoted the activation and hydrogenation of the C=O bond, producing deoxygenated aromatic compounds. Newman et al. [17] also reported a strong effect of the support on the selectivity to deoxygenated products for HDO of phenol in the liquid phase over Ru/SiO_2, Ru/Al_2O_3, Ru/C and Ru/TiO_2. The authors proposed that the strong interaction between the Ti^{3+} species formed during the reduction and the oxygen of the phenol promoted C–O bond cleavage, producing benzene. Chen and Pacchioni [18] carried out DFT analysis to investigate the HDO of phenol over Ru supported on the anatase TiO_2 (101) surface. The results showed that the energy barrier for C–O bond scission was decreased in the presence of Ti^{3+} species.

However, the role of reduced defects (e.g., oxygen vacancies or their associated Type II bridging OH groups) of the support in the HDO reaction pathway is controversial. First, the extent of TiO_2 reduction is very limited in comparison with materials such as ceria and ceria-mixed oxides. In this case, the addition of zirconia to ceria structure enhances significantly the density of oxygen vacancies of the support. For example, the high mobility of oxygen vacancies may assist in the catalytic reaction. Schimming et al. [19] tested a series of $Ce_xZr_{1-x}O_2$ catalysts with different Ce/Zr ratios for the HDO of guaiacol. The results demonstrated that the activity depended on the concentration of oxygen vacancies. The guaiacol molecule adsorbed on the oxygen vacancies that promoted the activation of the C–O bond. Wang et al. [20] also observed an improvement in the catalytic activity for the HDO of p-cresol when CeO_2 and ZrO_2 were added to a Pt/Al_2O_3 catalyst. The authors attributed this result to the creation of oxygen vacancies. In contrast, de Souza et al. [15] and Mortensen et al. [21] did not observe the existence of a correlation between the deoxygenation activity and the oxygen vacancy concentration for the HDO of phenol over Pd and Ni catalysts supported on different materials.

Therefore, the aim of this work is to study the performance of $Pd/Ce_xZr_{1-x}O_2$ catalysts with different compositions of Ce/Zr to shed light on the role of reduced defects of the support on the activity and stability of the catalyst for HDO of phenol. In situ X-ray absorption spectroscopy and XPS were used to follow the formation of Ce^{3+} species during reduction, which may aid in elucidating its role in the reaction mechanism.

2. Experimental section

2.1. Catalyst preparation

$Ce_xZr_{1-x}O_2$ (x = 0.00; 0.10; 0.25; 0.50; 0.75; 1.00) was synthesized by the precipitation or coprecipitation method. For CeO_2, a solution of ammonium cerium (IV) nitrate ($(NH_4)_2Ce(NO_3)_6$, Sigma-Aldrich) was added slowly to a solution of 4.0 mol/L ammonium hydroxide (NH_4OH, Vetec) at room temperature, and kept under vigorous stirring for 30 min. The resulting precipitate was filtered and washed with distilled water until a pH of 7 was reached. Then, the solid was dried at 383 K for 12 h and calcined under dry air flow at 773 K (heating ramp 5 K/min) for 6 h. $Ce_xZr_{1-x}O_2$ mixed oxides with different Ce/Zr molar ratios were prepared by coprecipitation using zirconyl nitrate and ammonium cerium (IV) nitrate solutions, following the same procedure as previously described for CeO_2. Tetragonal zirconia was supplied by Saint-Gobain NorPro. The catalysts (Pd/CeO_2, $Pd/Ce_{0.75}Zr_{0.25}O_2$, $Pd/Ce_{0.50}Zr_{0.50}O_2$, $Pd/Ce_{0.25}Zr_{0.75}O_2$, $Pd/Ce_{0.10}Zr_{0.90}O_2$, Pd/ZrO_2) with nominal Pd loading of 2 wt % were prepared by incipient wetness impregnation of the supports with an aqueous solution of $Pd(NO_3)_2$ (solution of 20% Pd in nitric acid, Umicore). The volume of solution used was determined by the wet point of the respective supports: 0.2 mL/g for Pd/CeO_2, $Pd/Ce_{0.75}Zr_{0.25}O_2$ and 0.4 mL/g for $Pd/Ce_{0.50}Zr_{0.50}O_2$, $Pd/Ce_{0.25}Zr_{0.75}O_2$, $Pd/Ce_{0.10}Zr_{0.90}O_2$, Pd/ZrO_2. After impregnation, the powder was dried in air at 393 K for 12 h and then calcined at 673 K (heating ramp 2 K/min) for 3 h under synthetic air flow (50 mL/min).

2.2. Catalyst characterization

The chemical composition of each sample was determined by X-ray fluorescence (XRF) using a Wavelength Dispersive X-Ray Fluorescence Spectrometer (WD-XRF) S8 Tiger, Bruker with a rhodium tube operated at 4 kW. The analyses were performed with the samples (300 mg) in powder form using a semiquantitative method (QUANT-EXPRES/Bruker). Specific surface areas of the samples were measured using a Micromeritics ASAP 2020 analyzer by N_2 adsorption at the boiling temperature of liquid nitrogen. The X-ray powder diffraction (XRD) patterns were obtained on a BRUKER D8 Advancer diffractometer using Cu Kα radiation over a 2θ range of 10-90° at a scan rate of 0.04°/step and a scan time of 1 s/step. The Raman spectra were recorded using a Horiba LabRam HR-UV800/Jobin-Yvon Spectrometer, equipped with He-Ne laser (λ = 632 nm) with 10 mW of intensity, a CCD detector and an Olympus BX41 microscope with objective lens of 100 × .

The density of acid sites of the catalysts was investigated by temperature-programmed desorption of ammonia (NH_3-TPD). The samples (350 mg) were reduced at 573 K for 1 h under a flow of H_2 of 60 mL/min and then purged in He flow for 30 min. After reduction, the sample was cooled to 423 K and the hydrogen flow was switched to a mixture containing 4% NH_3 in He (30 mL/min) for 30 min. The physisorbed ammonia was flushed out with flowing He for 1 h. Then, the catalyst was heated at 20 K/min under He to 773 K.

DRIFTS of adsorbed cyclohexanone was carried out to investigate the oxophilic sites using a Nicolet Nexus 870 instrument with a DTGS-TEC detector and a Thermo Spectra-Tech reaction chamber with ZnSe windows. The samples were reduced under the same conditions used in the NH_3-TPD experiments. Then, the catalyst was cooled to 323 K, He was flowed through a bubbler containing cyclohexanone at 60 mL/min, and spectra were recorded at 323 and 373 K. Peak fitting was performed on the band corresponding to adsorbed cyclohexanone by using Gaussian peaks and the nonlinear generalized reduced gradient (GRG) algorithm.

Because H_2 and CO chemisorb to the surfaces of both active metals and active oxides [22] (e.g., partially reducible oxides, where hydrogen forms bridging OH groups and CO forms adsorbed formate and related species), an alternate method for determining metal dispersion is often used. In the case of Pd and Ce-containing supports, determining Pd dispersion by transmission electron microscopy is also problematic, because of the low contrast between metal and support. One way to circumvent the limitations of H_2 and CO chemisorption and TEM techniques is to select a metal-catalyzed probe reaction, and in this work, cyclohexane dehydrogenation was used. For the purpose of calibration, metal dispersions were ascertained by CO chemisorption for Pd supported on less active supports such as Pd/SiO_2, Pd/Al_2O_3 and Pd/ZrO_2 [15]. Then, this was correlated with the cyclohexane dehydrogenation rate. Cyclohexane dehydrogenation was performed using a fixed-bed reactor at atmospheric pressure over fresh catalyst. The fresh samples were first reduced at 573 K for 1 h and then cooled to the cyclohexane dehydrogenation reaction temperature (543 K). The reaction mixture (WHSV = 52 h^{-1}) was fed into the reactor after bubbling H_2 through a saturator containing cyclohexane kept at 285 K (H_2/C_6H_{12} = 13.2). The exit gases were analyzed using an Agilent Technologies 7890 A/5975C GCMS, using an HP-Innowax capillary column and a flame-ionization detector (FID).

The reduced samples were analyzed with an aberration corrected Scanning Transmission Electron Microscope (STEM) (JEOL JEM-ARM200 F) operated at 200 kV. The instrument is equipped with CEOS GmbH double-hexapole aberration corrector for the probe-forming lens, which allows imaging with ˜0.8 nm resolution in scanning transmission electron microscopy (STEM) mode. The images were acquired on an HAADF detector with beam convergence of 27.5 mrad and collection angle of 68–280 mrad. Elemental analysis was performed using Energy Dispersive Spectroscopy (EDS) with a high collection angle SSD (˜0.7

srad, JEOL Centurio). The data were acquired and evaluated with the NSSThermo Scientific software package due to the instrument upgrade. In general, the STEM sample preparation involved mounting powder samples on copper grids covered with lacey carbon support films, and then immediately loading them into the STEM airlock to minimize exposure to atmospheric O_2.

In situ XAS experiments were performed at the D08B-XAFS – 2 beamline of the Brazilian Synchrotron Light Source (LNLS, Campinas). Typically, wafers containing pressed mixtures of the sample with boron nitride as a binder were then placed into a sample holder located inside a quartz tubular reactor. XANES spectra were successively recorded around the Ce L_{III}-edge (E_0 = 5.723 keV), while the sample underwent the following treatment: (i) reduction under a 5% H_2/He mixture from 298 to 573 K (10 K/min), remaining at this temperature for 1 h; and (ii) flowing a mixture containing 2.2%H_2/1.56%H_2O in He that was obtained by bubbling H_2 through a saturator containing water at 293 K. Data reduction was made using the ATHENA software package. The background subtracted, normalized XANES spectra were then truncated over a suitable energy range (80 eV above the absorption edge). The fractions of Ce^{4+} and Ce^{3+} during the different treatments of the sample were estimated by linear combination of normalized Ce LIII edge XANES spectra (LC-XANES) within the 5.70–5.76 keV energy range, using CeO_2 and $Ce(NO_3)_3.6H_2O$ as references for Ce^{4+} and Ce^{3+}, respectively.

XPS was used to evaluate the surface composition of the fresh and reduced catalysts. The fresh samples were measured in a K-Alpha$^+$ (Thermo Scientific) apparatus, using monochromatic Al K-α radiation (1486.7 eV), with beam size of 400 µm and a CCD detector. To avoid charging effects, a flood gun was used employing low energy electrons (less than 1 eV) during analysis. Binding energies (BE) were referred to the C 1 s line of carbon contaminant at 284.8 eV with an uncertainty of ± 0.1 eV. The electron analyzer was operated in fixed pass energy mode (40 eV). The fresh samples were powdered onto a carbon tape and loaded into a high vacuum chamber (˜10-8 mbar). Fitting and deconvolution were performed with CasaXPS software, using a 30/70 Gaussian/Lorentzian function. The reduced samples were analyzed in a SPECSLAB II PHOIBOS (Specs) apparatus, equipped with a pre-chamber that allows heating and gas feeding, employing non-monochromatic Al K-α radiation and channeltron detection. The spectra acquisition was performed in the same form of the described for fresh samples. For reduction, the catalysts were pressed to form a pellet and loaded into the high-temperature chamber and reduced at 573 K by flowing a 5% H_2/He mixture for 3 h; afterwards, the samples were cooled under He, and degassed prior to being transferred to the analysis chamber (˜10-8 mbar).

The main causes of catalyst deactivation were investigated by in situ DRIFTS under reaction conditions. DRIFTS spectra were recorded using a Nicolet Nexus 870 spectrometer equipped with a DTGS-TEC detector. A Thermo Spectra-Tech cell capable of high pressure/high temperature operation and fitted with ZnSe windows served as the reaction chamber for in-situ adsorption and reaction measurements. To reduce the sample, H_2 was flowed at 573 K for a period of 1 h and then a background spectrum was recorded. The scan resolution was 4 cm^{-1} and 512 scans were taken. Then, pure H_2 was flowed through a bubbler containing phenol at 60 mL/min and several spectra were recorded during the steady-state HDO reaction at 573 K for 6 h.

2.3. Catalytic activity

HDO of phenol in the vapor-phase was carried out in a fixed-bed quartz reactor, operating at atmospheric pressure of H_2 and 573 K. Diffusion limitations were ruled out based on the method of Madon and Boudart [23]. Catalyst particles (53–106 µm) were diluted with SiC particles (200–450 µm, mass ratio: SiC / catalyst = 3.0) to avoid localized heating. Prior to the reaction, the catalyst was reduced in situ under pure hydrogen (60 mL/min) at 573 K for 1 h. The reactant mixture was obtained by flowing H_2 through the saturator containing phenol, which was kept at the specific temperature required to obtain the desired H_2/phenol molar ratio (about 60). To avoid condensation, all lines were heated to 523 K.

In one set of experiments, catalysts were tested at different W/F ratios, where W/F is the ratio of catalyst amount in grams to the mass flow rate of the feed in grams per hour, by varying catalyst amount (ranging from 2.5 to 150 mg). Initial conversion was measured after 5 min to minimize the effect of catalyst deactivation. In another set of experiments, 150 mg of catalyst and a total flow rate of 60 mL/min were used for all tests to assess catalyst stability during 20 h of reaction. The reaction products were analyzed using an Agilent Technologies 7890 A/5975C GCMS, equipped with a HP-Innowax capillary column and a flame-ionization detector (FID). The product yield and selectivity for each product were calculated as follows:

$$yield\,(\%) = \frac{mol\ of\ product\ produced}{mol\ of\ phenol\ fed} \times 100 \quad (1)$$

$$Selectivity\ (\%) = \frac{mol\ of\ product\ produced}{mol\ of\ phenol\ consumed} \times 100 \quad (2)$$

Catalyst stability was calculated by Eq. (3), assuming first-order kinetics for deactivation:

$$Stability = Ln(1 - X_{(tf)})/Ln(1 - X_{(t0)}) \quad (3)$$

Where $X_{(tf)}$ is the final conversion and $X_{(t0)}$ is the initial conversion.

3. Results and discussion

3.1. Catalyst characterization

Table 1 summarizes the chemical composition and the surface area of the samples. The Pd content measured by XRF was close to the nominal value (2 wt%) for all samples. Considering the Ce and Zr loadings, the molar composition of the samples was close to the expected value. Pd/CeO_2 and Pd/ZrO_2 samples showed specific surface areas of 56 and 102 m^2/g, respectively. The addition of zirconia to ceria significantly increased the surface area (90-114 m^2/g). Doping ceria with Zr improves its thermal stability during calcination, which enhances the specific surface area of the mixed oxides [24,25].

Raman spectroscopy was used to investigate the effect of Zr addition on the structure of the $Ce_xZr_{1-x}O_2$ supports. The Raman spectra of $Ce_xZr_{1-x}O_2$ are shown in Fig. 1. The Raman spectrum of CeO_2 exhibits a band at 464 cm^{-1} that is attributed to the symmetric stretching of Ce—O bonds for a metal oxide with cubic fluorite structure (Fm3m) [26]. For $Ce_{0.75}Zr_{0.25}O_2$ and $Ce_{0.50}Zr_{0.50}O_2$ samples, the addition of Zr decreases the intensity of this band that is also broadened and shifted to higher wavenumbers, and shoulders appears at 300 and 630 cm^{-1}. The enlargement and displacement are associated with the deformation of the lattice structure due to the substitution of Ce^{4+} cation (0.097 nm) by Zr^{4+} (0.084 nm) that has a smaller ionic radius, reducing the length of the Me-O bond of the cubic structure (Fm3m) [27]. Further increasing Zr content induces significant changes in the spectra. For $Ce_{0.25}Zr_{0.75}O_2$ and $Ce_{0.10}Zr_{0.90}O_2$ samples, new bands appear at 148,

Table 1
BET surface area and chemical composition of the samples determined by XRF.

Catalyst	(wt.%)			Molar composition (%)[a]	Surface area (m^2/g)
	Pd	CeO_2	ZrO_2		
Pd/CeO_2	2.2	97.8	–	Pd/CeO_2	56
$Pd/Ce_{0.75}Zr_{0.25}O_2$	2.1	76.3	21.6	$Pd/Ce_{0.72}Zr_{0.28}O_2$	90
$Pd/Ce_{0.50}Zr_{0.50}O_2$	1.8	52.4	45.7	$Pd/Ce_{0.45}Zr_{0.55}O_2$	102
$Pd/Ce_{0.25}Zr_{0.75}O_2$	1.9	31.6	66.3	$Pd/Ce_{0.25}Zr_{0.75}O_2$	114
$Pd/Ce_{0.10}Zr_{0.90}O_2$	1.9	12.9	85.2	$Pd/Ce_{0.10}Zr_{0.90}O_2$	97
Pd/ZrO_2	2.1	–	97.9	Pd/ZrO_2	102

[a] Ce and Zr molar composition determined by XRF.

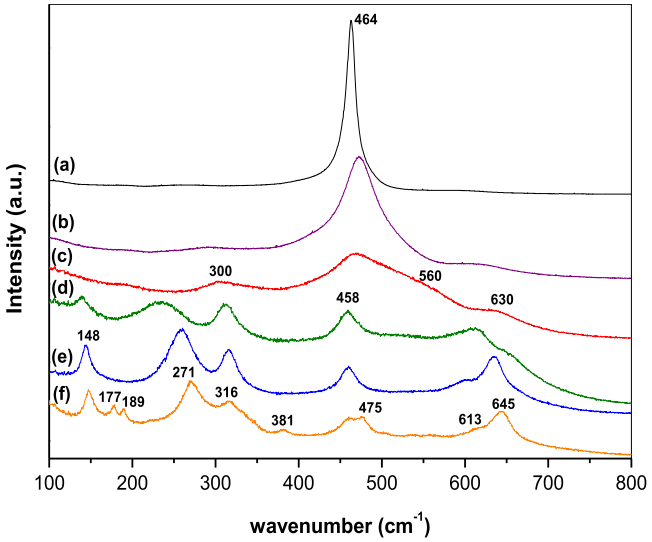

Fig. 1. Raman spectra of the supports (a) CeO_2; (b) $Ce_{0.75}Zr_{0.25}O_2$; (c) $Ce_{0.50}Zr_{0.50}ZrO_2$; (d) $Ce_{0.25}Zr_{0.75}O_2$; (e) $Ce_{0.10}Zr_{0.90}O_2$; (f) ZrO_2.

260, 315, 458, 598 e 636 cm^{-1}, which are characteristic of a tetragonal structure (P42/nmc) [28].

Fig. 2 shows the X-ray diffraction patterns for calcined samples. The diffractograms of Pd/CeO_2 and Pd/ZrO_2 exhibit lines characteristic of cubic (JCPDS 34-0394) and tetragonal (JCPDS 50–1089) structure, respectively. The addition of Zr to ceria shifted the ceria lines to higher 2θ positions. According to the literature [24,29,30], the shift in the lines characteristic of ceria to higher 2θ with the addition of Zr indicates the incorporation of Zr into the ceria lattice and the formation of a CeZr solid solution. $Ce_xZr_{1-x}O_2$ solid solution with cubic structure is formed between x = 0.5 to 1.0, whereas a tetragonal $Ce_xZr_{1-x}O_2$ solid solution is obtained for x < 0.5 [31,32]. This result agrees very well with the Raman spectra obtained (Fig. 1). From Fig. 2b, it is clear that the line is symmetrical for all samples, indicating the formation of a homogeneous solid solution with the expected composition. The CeO_2 lattice constant *a* was also calculated from the (111) reflections and is listed in Table 2. The calculated value for CeO_2 is close to the nominal one [33]. Furthermore, the addition of Zr to ceria decreased the lattice parameter from 5.4001 Å (Pd/CeO_2) to 5.2738 Å ($Pd/Ce_{0.50}Zr_{0.50}O_2$). For $Ce_{0.25}Zr_{0.50}O_2$; $Ce_{0.10}Zr_{0.90}O_2$ and ZrO_2 supports with tetragonal structure, the lattice parameter *a* varied from 3.7655 to 3.6102 Å.

According to the literature, CeZr solid solutions exhibit higher oxygen mobility than CeO_2 [25]. In order to measure the concentration of reduced defects of the $Pd/Ce_xZr_{1-x}O_2$ catalysts, in situ XANES and XPS experiments were carried out.

Figs. 3 and 4a show Ce L_{III}-edge XANES spectra of Pd/CeO_2 and $Pd/Ce_{0.25}Zr_{0.75}O_2$ catalysts, respectively, recorded during reduction under 5% H_2/He mixture from 293 to 573 K (black curves) and under the mixture containing water (orange curves). The spectra of the other catalysts are presented in the Supplementary material (Fig. S1-S3). For the calcined samples, there are four peaks attributed to Ce^{4+} (A and B), Ce^{3+} (C) and a pre-edge peak (D) (Fig. 3b and 4 b) [34,35]. The peaks A and B are the most intense ones, indicating that the calcined samples contain a higher fraction of Ce^{4+} species. The XANES spectra of Pd/CeO_2 catalyst remained unchanged when the temperature was increased from 298 to 573 K under 5% H_2/He mixture. There are no significant changes on XANES spectra during reduction for 1 h. This result indicates that the reducibility of Pd/CeO_2 catalyst is low, which is likely due to the low reduction temperature (573 K). For $Pd/Ce_{0.25}Zr_{0.75}O_2$ catalyst, the XANES spectra significantly changed during reduction with a significant increase in the intensity of the peak C, which suggests the progressive reduction of Ce^{4+} to Ce^{3+}. There is a further reduction when the catalyst is heated for 1 h.

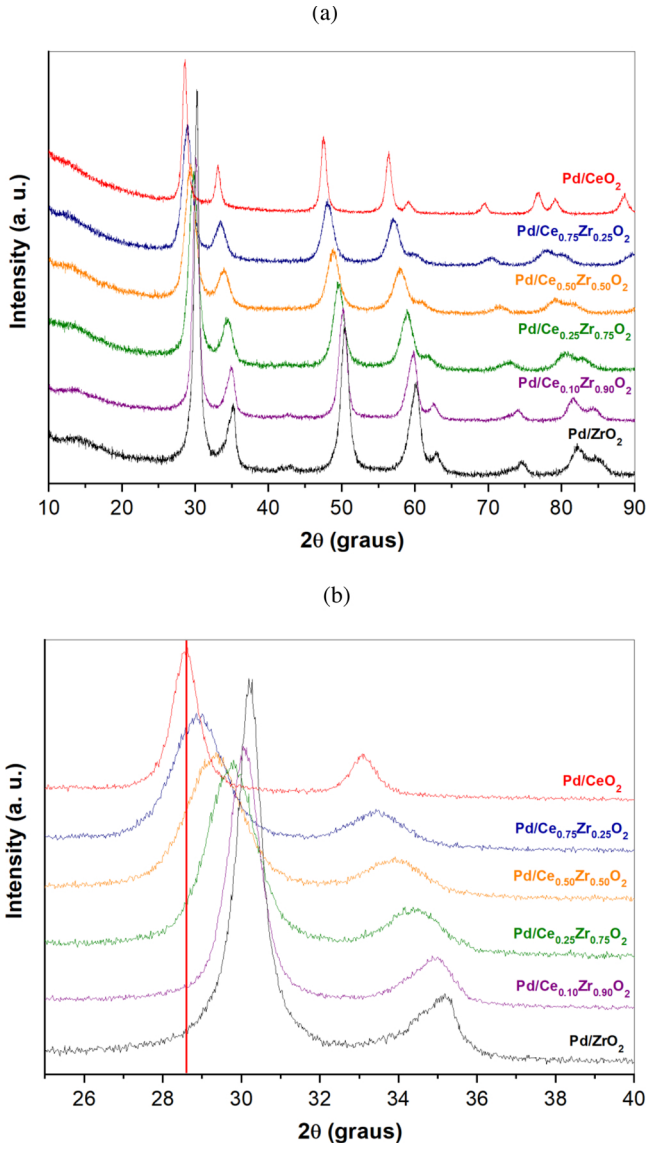

Fig. 2. X-ray diffraction patterns for $Pd/Ce_xZr_{1-x}O_2$ samples (x = 0.00; 0.10; 0.25; 0.50; 0.75; 1.00) between: (a) 2θ = 10 and 90°; (b) 2θ = 25 and 40°.

Table 2
Lattice parameter and Ce^{3+} molar fraction calculated by the linear combination of Ce L_{III}-edge XANES spectra after reduction at 573 K.

Catalyst	Lattice parameter[a] (Å)		Ce^{3+} molar fraction (%)
	a	c	
Pd/CeO_2	5.4001	–	0.10
$Pd/Ce_{0.75}Zr_{0.25}O_2$	5.3432	–	0.28
$Pd/Ce_{0.50}Zr_{0.50}O_2$	5.2738	–	0.48
$Pd/Ce_{0.25}Zr_{0.75}O_2$	3.7655	4.9565	0.55
$Pd/Ce_{0.10}Zr_{0.90}O_2$	3.7148	4.9573	0.37
Pd/ZrO_2	3.6102	5.1670	0.00

[a] The lattice parameter of CeO_2, $Ce_{0.75}Zr_{0.25}O_2$ and $Ce_{0.5}Zr_{0.5}O_2$ supports was calculated considering a cubic structure. For $Ce_{0.25}Zr_{0.50}O_2$; $Ce_{0.10}Zr_{0.90}O_2$ and ZrO_2 supports was considered a tetragonal structure.

Changes in the concentrations of Ce^{4+} and Ce^{3+} species during reduction calculated by the linear combination of Ce L_{III}-edge XANES spectra of references are shown in Fig. 3c and 4 c. All the calcined samples contain mainly Ce^{4+}, regardless of the Ce/Zr ratio. The reduction of Ce^{4+} to Ce^{3+} species began at different temperatures,

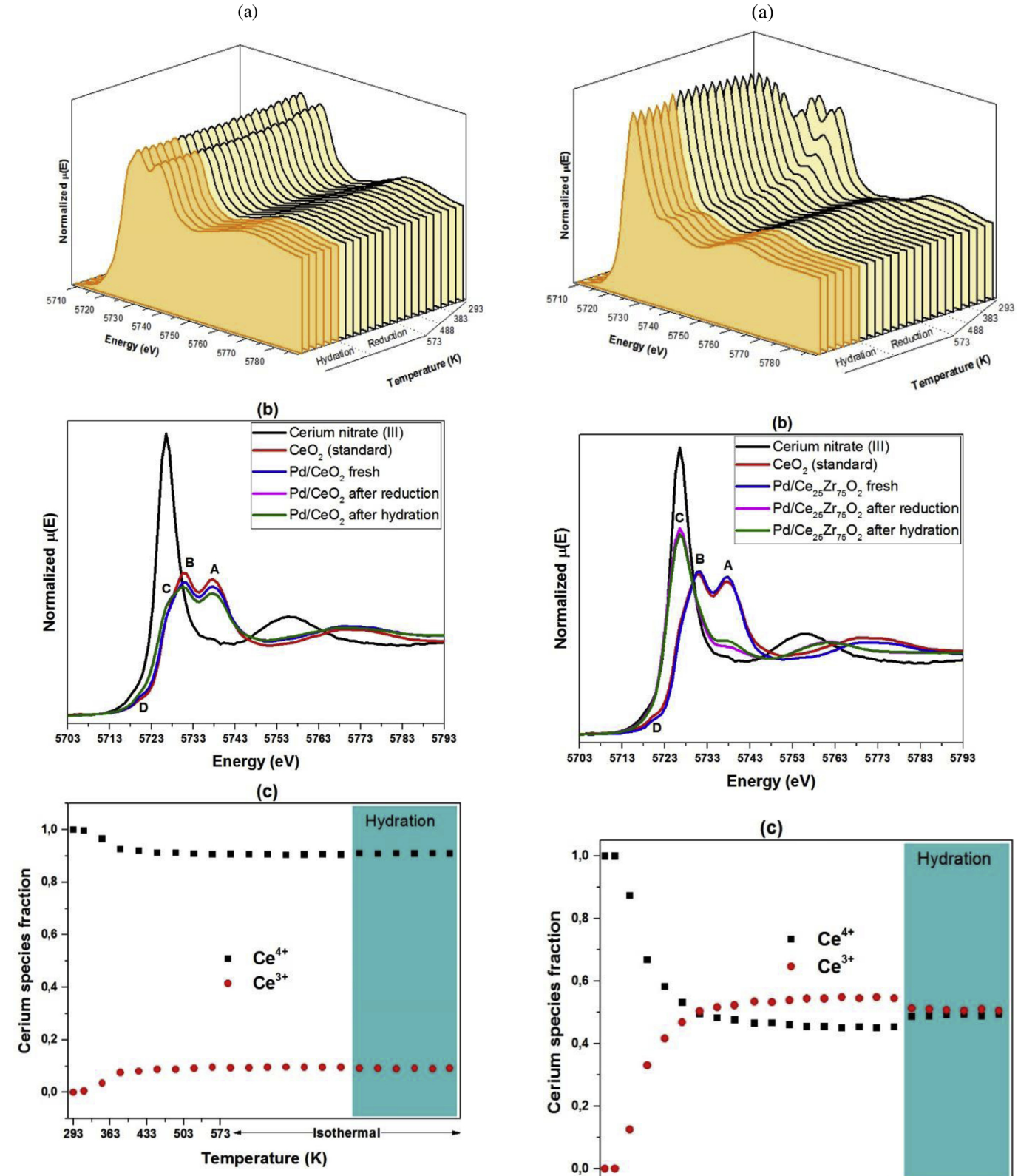

Fig. 3. (a) in situ XANES spectra at Ce L_{III}-edge of Pd/CeO_2 under different treatments (reduction at 573 K under 5% H_2/He mixture, hydration at 573 K under H_2 and H_2O mixture); (b) XANES spectra at specific temperatures: fresh sample (blue curve); after reduction at 573 K (pink curve); after hydration (green curve); and references compounds; (c) Linear combination of XANES spectra of Pd/CeO_2 considering CeO_2 and cerium nitrate as references (For interpretation of the references to colour in this figure legend, the reader is referred to the web version of this article).

(caption on next page)

depending on the Zr content. Furthermore, the extent of reduction increased as the Zr content increased and achieved a maximum for the $Pd/Ce_{0.25}Zr_{0.75}O_2$ catalyst (Table 2).

Fig. 4. (a) in situ XANES spectra of $Pd/Ce_{0.25}Zr_{0.75}O_2$ under different treatments (reduction at 573 K under 5% H_2/He mixture, hydration at 573 K under H_2 and H_2O mixture); (b) XANES spectra at specific temperatures: fresh sample (blue curve); after reduction at 573 K (pink curve); after hydration (green curve); and references compounds; (c) Linear combination of XANES spectra of $Pd/Ce_{0.25}Zr_{0.75}O_2$ considering CeO_2 and cerium nitrate as references (For interpretation of the references to colour in this figure legend, the reader is referred to the web version of this article).

Then, the mixture containing H_2 and H_2O was flowed through the sample for 1 h. The XANES spectra of Pd/CeO_2 catalyst remained unchanged and similar to the spectrum of the reduced catalyst after 1 h. However, the XANES spectra underwent changes when $Pd/Ce_xZr_{1-x}O_2$ catalysts were treated with water. The intensity of the peak C slightly decreased, indicating that Ce^{3+} species were partially oxidized. When the mixture containing water was flowed through the catalysts, it was noticed a small increase in the fraction of Ce^{4+} species that followed the order: $Pd/Ce_{0.10}Zr_{0.90}O_2 > Pd/Ce_{0.25}Zr_{0.75}O_2 > Pd/Ce_{0.50}Zr_{0.50}O_2 \approx Pd/Ce_{0.75}Zr_{0.25}O_2 > Pd/CeO_2$.

The XPS spectra of Pd 3d, Zr 3d, Ce 3d and O 1 s core levels of the reduced samples are shown in supplementary material (Fig. S4). The analysis of the Pd 3d spectra is rather complicated due to the overlapping with the more intense Zr 3p doublet, which hinders the identification of palladium oxide and metallic palladium in the spectra of the catalysts supported on ZrO_2 and mixed oxides rich in zirconia. The catalysts containing zirconia showed the Zr $3d_{5/2}$ and $3d_{3/2}$ levels with an energy gap of 2.4 eV between them, which indicate the presence of ZrO_2-like species.

The Ce 3d photoelectron spectra of $Pd/Ce_xZr_{1-x}O_2$ catalysts shows two sets of multiplets u and v, corresponding to the cerium $3d_{3/2}$ and $3d_{5/2}$ core levels respectively. u''' and v''' are assigned to the $3d^94f^0$ photoemission final state while v and v'' (u and u'') are due to a mixing of the $3d^94f^2$ and $3d^94f^1$ final states. The v' and u' lines indicate the presence of Ce^{3+} ions [36]. Pd/CeO_2 sample exhibits a typical spectrum reported in the literature for ceria corresponding mostly to the presence of Ce^{4+} ions [37,38]. Increasing the Zr content increased significantly the intensity of v' and u' lines, indicating that the incorporation of Zr into the ceria lattice led to the reduction of Ce^{4+} to Ce^{3+} and the creation of oxygen vacancies on the surface. The $Ce^{3+}/(Ce^{3+}+Ce^{4+})$ ratio increased from 0.06 (Pd/CeO_2) to 0.44 ($Pd/Ce_{0.25}Zr_{0.75}O_2$) and then decreased to 0.35 ($Pd/Ce_{0.10}Zr_{0.90}O_2$). The fraction of Ce^{3+} ions on the surface of reduced samples slightly increased from 0.06 to 0.07 and then decreased to 0.01 when the Zr content increased from 0.00 to 0.90. In addition, the reduction led to an important enrichment of Zr on the surface, mainly on the samples containing lower Zr content (Table 3).

Recently, DRIFTS experiments of adsorbed pyridine on Pd/CeO_2 and $Pd/Ce_{0.5}Zr_{0.5}O_2$ catalysts revealed only the presence of Lewis acid sites [15]. In order to determine the strength and the density of these Lewis acid sites, NH_3-TPD was carried out and the NH_3-TPD profiles of $Pd/Ce_xZr_{1-x}O_2$ catalysts are shown in Fig. S5. Several desorption peaks were observed in the range of 300 to 800 K, indicating a distribution of acid sites with different strengths. Curve fitting was performed using Gaussian peaks to represent the different strengths of acid sites. Good fits were obtained, and results are quantified in Table S1. The increase in the Zr content led to an increase in the fraction of strong acid sites. The total amount of acid sites of all catalysts was also calculated from NH_3-TPD profiles and the results are reported in Table 4. Increasing the zirconia content continuously increased the number of acid sites.

Table 4
Total amount of ammonia desorbed, reaction rate of dehydrogenation of cyclohexane (DHO) and Pd dispersion of fresh catalysts.

Catalyst	Ammonia desorbed ($\mu mol.\ g_{cat}^{-1}$)	Rate of DHO ($mmol.\ g_{Pd}^{-1}.\ min^{-1}$)	D[a](%)
Pd/CeO_2	59	0.20	23
$Pd/Ce_{0.75}Zr_{0.25}O_2$	101	0.23	25
$Pd/Ce_{0.50}Zr_{0.50}O_2$	157	0.35	33
$Pd/Ce_{0.25}Zr_{0.75}O_2$	230	0.37	35
$Pd/Ce_{0.10}Zr_{0.90}O_2$	269	0.51	50
Pd/ZrO_2	300	0.97	67

[a] Pd dispersion of the fresh catalysts calculated using the reaction rate of cyclohexane dehydrogenation (DHO).

STEM image of reduced catalysts with corresponding chemical mapping and EDX of selected area are shown in Fig. S6. The low Pd content and the poor contrast between Pd and support make difficult to distinguish between the Pd particles and the individual $CeZrO_2$ crystallites in the STEM images. Therefore, the size distribution analysis was not performed. The chemical mapping of the reduced and passivated sample gives an idea about the metal distribution. The chemical mapping images of $Pd/Ce_{0.10}Zr_{0.90}O_2$, $Pd/Ce_{0.50}Zr_{0.50}O_2$ and Pd/CeO_2 catalysts reveals Pd is well dispersed on the supports but some agglomerates are also found in some regions.

Then, the Pd dispersion was calculated using the dehydrogenation of cyclohexane (DHO) as a probe reaction and the results are reported in Table 4. The Pd dispersion increased as the Zr content increased from 23 to 67%.

DRIFTS experiments of adsorbed cyclohexanone were performed in order to measure the strength of the interaction between the oxygen from the carbonyl group and the oxophilic site. Fig. 5 shows the spectra obtained after desorption at 323 K in the region between $1600 - 1750\ cm^{-1}$, which corresponds to the C═O stretching mode. The entire spectrum for each cyclohexanone adsorption study is presented in supporting information (Fig. S7). Pd/CeO_2 exhibited two bands at 1711 and $1692\ cm^{-1}$ and a shoulder at $1680\ cm^{-1}$. The addition of zirconia decreased the intensity of the band at high wavenumber $1711\ cm^{-1}$ and led to the appearance of a new band at low wavenumber (around $1650\ cm^{-1}$). For Pd/ZrO_2 catalyst, the spectrum shows bands at 1707, 1685 and $1650\ cm^{-1}$.

In general, the band characteristic of the ν(C═O) stretching mode of carbonyl groups is located at $1715\ cm^{-1}$. Recently, we reported that the ν(C═O) of carbonyl groups is shifted to lower wavenumber due to the formation of cyclohexen-1-one and 2,4-cyclohexadien-1-one species [15]. The shift of the band characteristic of the ν(C═O) stretching mode of carbonyl band was attributed to the conjugation of the carbonyl group with the unsaturated ring. Corma et al. [39,40] proposed to use this shift to measure the strength of the interaction between the oxygen of phenolic compounds and the oxophilic sites. We applied this methodology to determine the oxophilicity of Pd based catalysts using

Table 3
The quantitative results of different atoms by XPS and peak-fitting results of Pd 3d, Zr 3d, Ce 3d and O 1 s spectra of the reduced samples.

Catalyst	Atomic composition (%)				Intensities ratios		
	Pd	Ce	Zr	O	$Ce^{3+}/(Ce^{3+}+Ce^{4+})$	Ce/(Ce + Zr)	Ce^{3+}/(Ce + Zr)
Pd/CeO_2	3.7	31.7	–	64.7	0.06	1.00	0.06
$Pd/Ce_{0.75}Zr_{0.25}O_2$	4.2	16.2	25.2	54.5	0.17	0.39	0.07
$Pd/Ce_{0.50}Zr_{0.50}O_2$	2.1	9.4	38.9	49.6	0.31	0.19	0.06
$Pd/Ce_{0.25}Zr_{0.75}O_2$	1.5	3.2	47.6	41.9	0.44	0.06	0.03
$Pd/Ce_{0.10}Zr_{0.90}O_2$	1.6	1.4	53.5	43.5	0.35	0.03	0.01

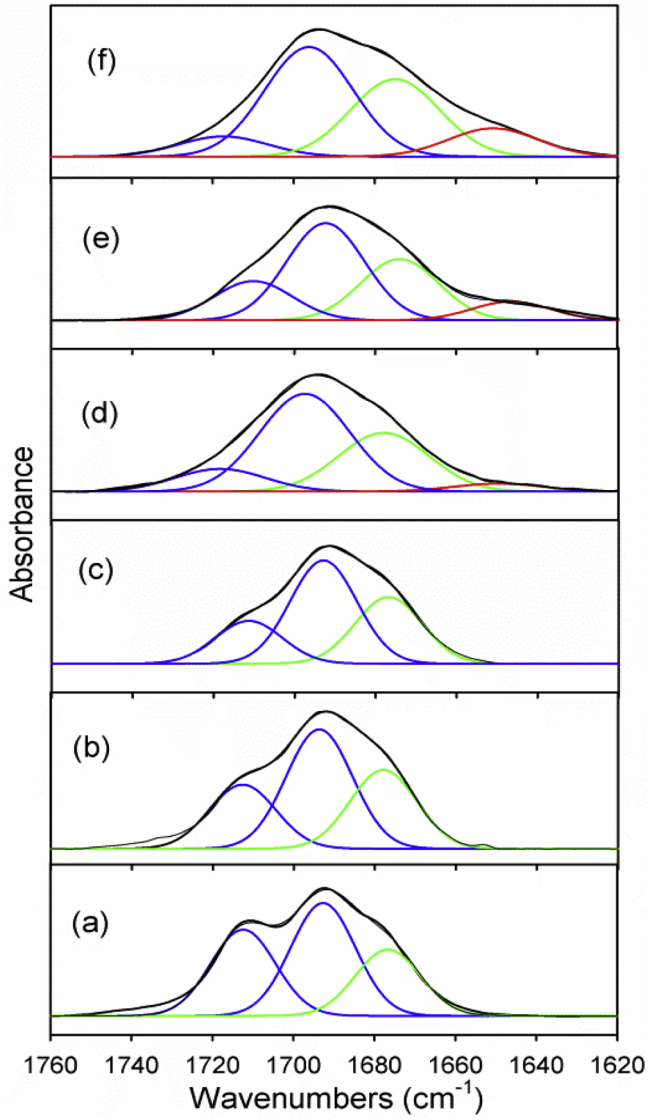

Fig. 5. Cyclohexanone spectra after desorption at 323 K over: (a) Pd/CeO_2; (b) $Pd/Ce_{0.75}Zr_{0.25}O_2$; (c) $Pd/Ce_{0.50}Zr_{0.50}O_2$; (d) $Pd/Ce_{0.25}Zr_{0.75}O_2$; (e) $Pd/Ce_{0.10}Zr_{0.90}O_2$; (f) Pd/ZrO_2. Blue curves: High wavenumber bands; green curves: medium wavenumber bands; red curves: low wavenumber bands (For interpretation of the references to colour in this figure legend, the reader is referred to the web version of this article).

Table 5
Distribution of the different regions of the band associated with ν(C═O) of cyclohexanone.

Catalyst	% Wavenumber bands		
	High $\geq$ 1695 cm^{-1}	Medium 1660 - 1695 cm^{-1}	Low 1620 - 1660 cm^{-1}
Pd/CeO_2	75.0	25.0	0.0
$Pd/Ce_{0.75}Zr_{0.25}O_2$	70.0	30.0	0.0
$Pd/Ce_{0.50}Zr_{0.50}O_2$	68.7	31.3	0.0
$Pd/Ce_{0.25}Zr_{0.75}O_2$	64.4	31.4	4.2
$Pd/Ce_{0.10}Zr_{0.90}O_2$	63.0	28.3	8.7
Pd/ZrO_2	55.1	32.9	12.0

different supports. The spectra of adsorbed cyclohexanone on Pd/CeO_2 and Pd/ZrO_2 catalysts were quite similar to the ones obtained in the present work. The cyclohexanone spectra were decomposed into three regions: high ($>$ 1695 cm^{-1}), medium (1660 − 1695 cm^{-1}), and low ($<$ 1660 cm^{-1}) wavenumbers. Pd/CeO_2 catalyst exhibited a high fraction of the band located in the high wavenumber region, whereas the Pd/ZrO_2 catalyst had a higher percentage in the medium/low wavenumber region, which was attributed to the higher oxophilicity of this material. This procedure was used in our work and the results obtained are reported in Table 5. The addition of zirconia to ceria led to a continuous increase in the fraction of bands located in the medium/low wavenumber region, as previously observed [15]. This result indicates that the addition of Zr promotes the interaction between the oxygen from the carbonyl group and metal cations.

3.2. HDO of phenol over $Pd/Ce_xZr_{1-x}O_2$ catalysts

The HDO of phenol over all supports not exhibit any significant activity even at high W/F (0.46 h). The phenol conversion and product yield as a function of W/F at 573 K over Pd/CeO_2, $Pd/Ce_{0.75}Zr_{0.25}O_2$, $Pd/Ce_{0.25}Zr_{0.75}O_2$, and Pd/ZrO_2 catalysts are shown in Fig. 6.

The main products formed were benzene, cyclohexanone (ONE), cyclohexanol (OL) as well as small amounts of cyclohexane for $Pd/Ce_xZr_{1-x}O_2$ catalysts. C_{12} hydrocarbons (biphenyl and cyclohexylbenzene) and C_{12} O-containing hydrocarbons (2-phenylphenol, 2-cyclohexylcyclohexan-1-one and 2-cyclohexylphenol) were also detected in small amounts at high conversion on Pd/ZrO_2 catalyst. However, product distribution significantly depended on the Ce/Zr molar ratio of the support and W/F.

At low W/F ($<$ 0.5 h), cyclohexanone was the main product formed for Pd/CeO_2. The addition of Zr increased the formation of benzene in this region. Higher formation of benzene only occurred at high conversions and small yields of cyclohexanol were also observed over these catalysts. For Pd/ZrO_2 catalyst, benzene was the main product over the whole range of W/F. In this case, only small yields of cyclohexanone and C_{12} hydrocarbons were observed. The formation of bicyclic hydrocarbons is likely due to the alkylation of phenolic and aromatic rings by cyclohexanone over Lewis acid sites [41].

The reaction rate of HDO of phenol was calculated and the selectivity of all catalysts was compared at low phenol conversion and these results are listed in Table 6.

The deoxygenation rate was approximately the same for Pd/CeO_2, $Pd/Ce_{0.75}Zr_{0.25}O_2$ and $Pd/Ce_{0.50}Zr_{0.50}O_2$ catalysts. However, the reaction rate significantly increased for catalysts with Zr content higher than 0.5. Pd/ZrO_2 catalyst exhibited the highest reaction rate that was about 30-fold higher than the one obtained for $Pd/Ce_{0.75}Zr_{0.25}O_2$. The reaction rates displayed the following trend: $Pd/ZrO_2 > > Pd/Ce_{0.10}Zr_{0.90}O_2 > Pd/Ce_{0.25}Zr_{0.75}O_2 > Pd/Ce_{0.50}Zr_{0.50}O_2 \approx Pd/Ce_{0.75}Zr_{0.25}O_2 \approx Pd/CeO_2$.

The product distribution varied significantly with the Ce/Zr molar ratio. Pd/CeO_2, $Pd/Ce_{0.75}Zr_{0.25}O_2$ and $Pd/Ce_{0.50}Zr_{0.50}O_2$ catalysts exhibited a high selectivity to cyclohexanone and cyclohexanol. Increasing the Zr content favored the formation of benzene and decreased the selectivity to cyclohexanone and cyclohexanol. Pd/ZrO_2 showed the highest selectivity to benzene without the formation of cyclohexanol. For instance, Pd/ZrO_2 catalyst showed selectivity to benzene that was 10-fold higher than that of either Pd/CeO_2 or $Pd/Ce_{0.75}Zr_{0.25}O_2$ catalysts. These results suggest that the Zr content on the mixed oxide significantly affects the deoxygenation activity and product distribution of the catalysts for HDO of phenol.

3.3. Effect of reduced defects of the support on the reaction pathway for HDO of phenol

Different proposals are found in the literature about the role of the support on the reaction mechanism of HDO of phenolic molecules. Several papers suggest that the acid sites of the support are responsible for the deoxygenation activity [3,4,21] whereas other ones propose that the oxophilic sites promote the formation of deoxygenated products [5–10,14–17]. There are also some authors that correlated the deoxygenation activity to the oxygen vacancies of the support [19,20].

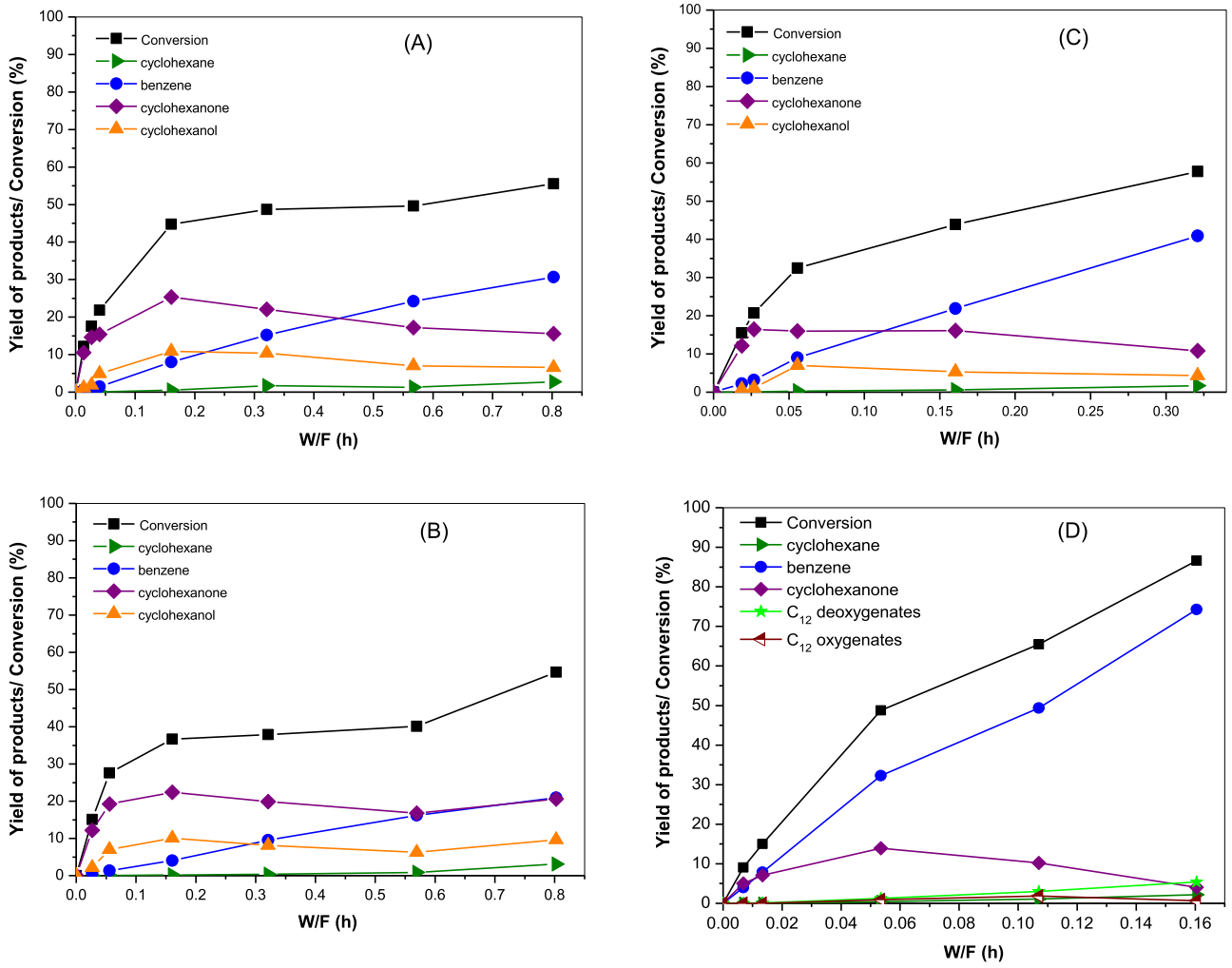

Fig. 6. Phenol conversion and products yield as a function of W/F over (A) Pd/CeO_2; (B) $Pd/Ce_{0.75}Zr_{0.25}O_2$; (C) $Pd/Ce_{0.25}Zr_{0.75}O_2$; (D) Pd/ZrO_2.

Table 6
Reaction rate of HDO of phenol and product distribution at low conversion.

Catalyst	Conversion (%)	Rate of HDO (mmol. $min^{-1}.g_{cat}^{-1}$)	Selectivity (%)		
			BZ	ONE	OL
Pd/CeO_2	12.2	0.09	4.4	86.3	9.3
$Pd/Ce_{0.75}Zr_{0.25}O_2$	15.1	0.04	4.7	80.7	14.6
$Pd/Ce_{0.50}Zr_{0.50}O_2$	13.9	0.09	4.6	84.6	10.9
$Pd/Ce_{0.25}Zr_{0.75}O_2$	15.5	0.19	14.5	78.5	4.9
$Pd/Ce_{0.10}Zr_{0.90}O_2$	11.9	0.43	18.0	80.1	1.9
Pd/ZrO_2	9.1	1.20	44.2	55.8	0.0

BZ: benzene; ONE: cyclohexanone; OL: cyclohexanol.

Fig. 7a shows the variation of benzene selectivity and the total amount of ammonia desorbed as a function of the zirconia content. The density of acid sites continuously increased with the Zr content but the selectivity to benzene did not follow the same trend. Therefore, there is no relationship between the selectivity to deoxygenated products and the density of acid sites. The same result was reported by de Souza et al. [15]. In this case, NH_3-TPD experiments showed that Pd/Al_2O_3 catalyst exhibited the highest density of Lewis acid sites whereas the highest selectivity to benzene was observed with Pd/ZrO_2 and Pd/TiO_2 catalysts. Mortensen et al. [21] also proposed that the density of acid sites of the support does not affect the activity for HDO of phenol in liquid phase over Ni supported catalysts.

The reduction of ceria-based supports is a complex process. Not only are oxygen vacancies produced, but Type II bridging OH groups are also formed; both are associated with Ce^{3+} sites on the surface. The Type II bridging OH are formed in one of two ways: (1) from the dissociation of water at O-vacancy sites (already Ce^{3+}), or (2) directly from dissociation of hydrogen on the metal and spillover to the support during activation, where O is replaced by OH, such that Ce^{4+} is converted to Ce^{3+} [42]. Thus, while Ce^{3+} cations at O-vacancies are exposed to reactants, Ce^{3+} cations associated with Type II bridging OH groups are not directly exposed to the reactants. Therefore, it is important to note that the determination of the concentration of Ce^{3+} species is a measurement of total reduced defect sites.

The selectivity to benzene and the fraction of Ce^{3+} species formed after reduction at 573 K, calculated by the linear combination of Ce L_{III}-edge XANES spectra, were plotted as a function of Zr content (Fig. 7b). Increasing the Zr content from x = 0.0 to 0.5 did not change the selectivity to benzene (which remained very low), whereas the fraction of Ce^{3+} species significantly increased from 0.10 to 0.55. Further increases in the Zr content led to a strong increase in the selectivity to benzene but the fraction of Ce^{3+} species went through a maximum and significantly decreased.

The XANES experiment gives information about the concentration of Ce^{3+} species in the bulk. The XPS results may provide the concentration of Ce^{3+} species on the surface of the catalyst. Then, the fraction of Ce^{3+} species on the reduced catalysts, as calculated from the XPS experiments, was compared to the selectivity to benzene (Fig. 7b). The fraction of Ce^{3+} species on the surface exhibited the same trend obtained by the XANES experiments, showing a maximum when the Zr loading increased. However, the selectivity to benzene remained

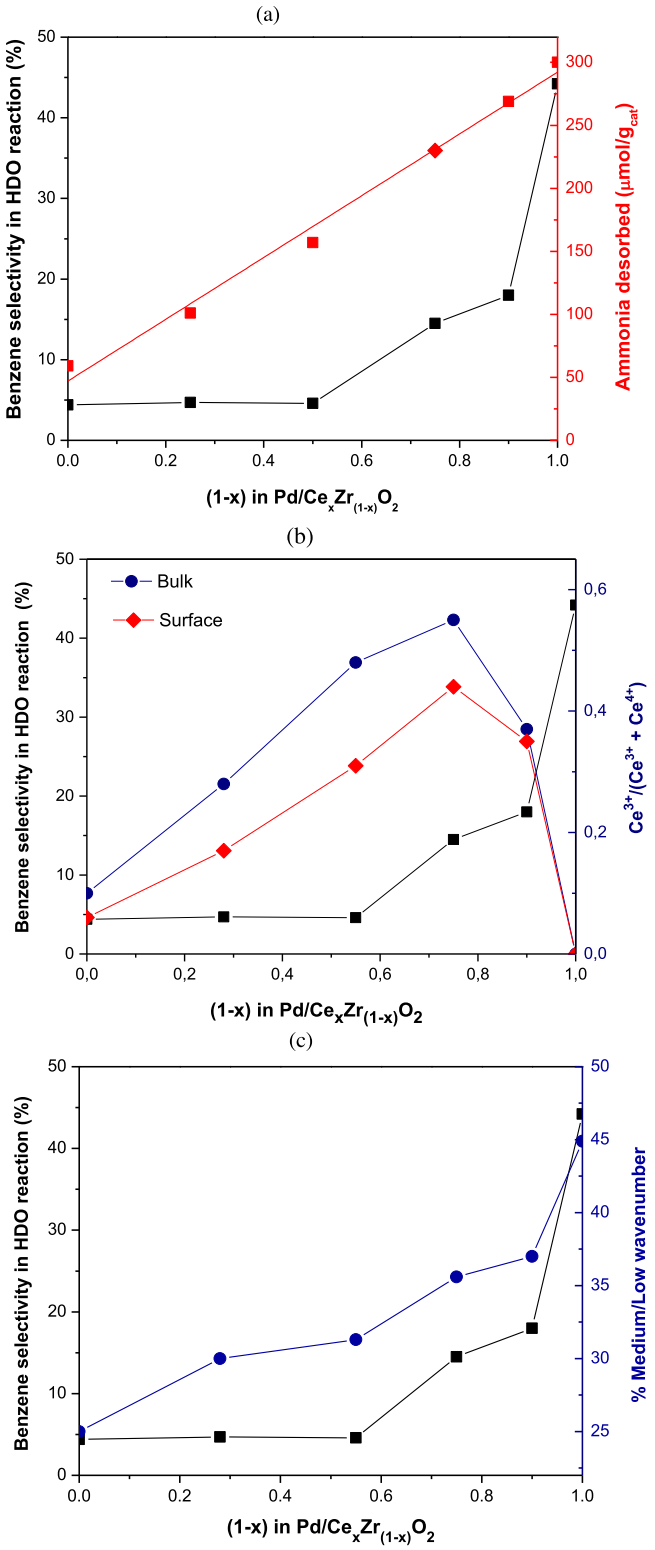

Fig. 7. (a) The selectivity to benzene for HDO reaction and the amount of ammonia desorbed as a function of Zr content; (b) The selectivity to benzene for HDO of phenol and the fraction of Ce^{3+} species calculated by the linear combination of Ce L_{III}-edge XANES spectra and XPS as a function of Zr content; (c) Selectivity to benzene and percentage of bands of cyclohexanone at medium/low regions of wavenumber as a function of Zr content.

constant up to 50% of Zr and then sharply increased as the Zr content further increased. These results demonstrate that there is no direct correlation between the density of reduced defect sites and the deoxygenation activity. In fact, the XANES experiment showed that the addition of water on the hydrogen flow only slightly changed the fraction of Ce^{3+} species (Figs. 3c and 4 c). This result indicates that the Type II bridging OH groups occupy the oxygen vacancies and ceria remains in the Ce^{3+} oxidation state. This means that the oxygen vacancies did not affect the deoxygenation activity.

These results agree very well with the work of de Souza et al. [15], who investigated the role of the oxygen vacancies for the HDO of phenol using IR of adsorbed CO. In order to measure the density of oxygen vacancies, they used the ratio between the intensities of the formate bands and the carbonyl bands on the metallic particles from DRIFTS spectra of adsorbed CO on different Pd-based catalysts. They reported the following order for this ratio: $Pd/CeZrO_2 > Pd/CeO_2 > Pd/ZrO_2 > > Pd/Al_2O_3 > Pd/TiO_2$. This result is in agreement with the literature that reports higher oxygen mobility for supports like ceria and ceria-zirconia mixed oxides. However, $Pd/CeZrO_2$ and Pd/CeO_2 catalysts exhibited lower activity to deoxygenation and selectivity to benzene than Pd/ZrO_2 and Pd/TiO_2 catalysts. This result suggested that there was no clear correlation between the concentration of oxygen vacancies on the supports and the deoxygenation activity of phenol over these Pd-based supported catalysts.

Recently, efforts point to a role played by oxophilic sites (i.e., unreduced metals and metal oxide cations from the supports) in facilitating the deoxygenation [7,8,17,43]. Bonding of phenol by its oxygen atom to such sites could promote the hydrogenation of the carbonyl group or even the direct C–O bond cleavage.

The term oxophilicity is often used to imply affinity to oxygen and oxygenated functional groups, such as −CO, −OH, R−O−R, etc., which are common in biomass-derived compounds. The metal oxophilicity is associated with the position of the d-band center relative to the Fermi level [44], which in turn depends on the metal type and the extent of coordination of the metal atoms. As the d-band center is closer to the Fermi level, the anti-bonding orbital of the hybridization between metal and oxygen is further away from the Fermi level and has low electron occupancy [45]. Therefore, the M–O bond becomes stronger and the metal is more oxophilic.

HDO of m-cresol in the gas phase was carried out over silica-supported catalysts (Pd, Pt, Rh, Ru, Ni, Fe, NiFe) [5,8]. The reaction mechanism depended on the type of the metal. DFT computational studies revealed that oxophilic metals such as Ru and Fe promote the deoxygenation, whereas tautomerization/hydrogenation is favored over less oxophilic metals (e.g., Pt, Pd). DFT calculations showed a general correlation between the energy barrier for direct deoxygenation and the oxophilicity of metal surfaces, taking into account the binding energy of oxygen to the metal surface. The higher strength of the interaction between oxygen from the carbonyl and Ru than Pt reduces the energy barrier for the deoxygenation pathway.

Teles et al. [46] studied the effect of metal type on the reaction mechanism for HDO of phenol over a series of silica-supported metal (Pd, Pt, Rh, Ru, Ni, Co) catalysts. Silica-supported Pt, Pd, and Rh favored the formation of hydrogenated products (cyclohexanone and cyclohexanol), whereas significant formation of hydrogenolysis products (C_5–C_6 hydrocarbons and methane) was observed over Co/SiO_2, Ni/SiO_2, and mainly Ru/SiO_2 catalysts. Therefore, the direct dehydroxylation of phenol followed by hydrogenolysis is favored over more oxophilic metals (Ru, Co, and Ni). The authors established a correlation between the oxophilicity of the metal and deoxygenation activity based on its ability to bind with oxygen from the carbonyl group. Increasing the binding energy of atomic oxygen led to an increase in the selectivity to deoxygenated products. The highest selectivity to deoxygenated products was obtained for Ru-based catalyst, a metal with which the oxygen binds strongly. On the other hand, Pd/SiO_2 catalyst did not exhibited the formation of deoxygenated products due to its low binding energy of atomic oxygen. These results reveal that the more oxophilic the metal favors the selectivity to deoxygenated products.

However, the order observed for the selectivity to deoxygenated products for zirconia-supported catalysts [10] was not the same as that obtained for the silica-supported catalysts [46]. For instance, Pt and Pd

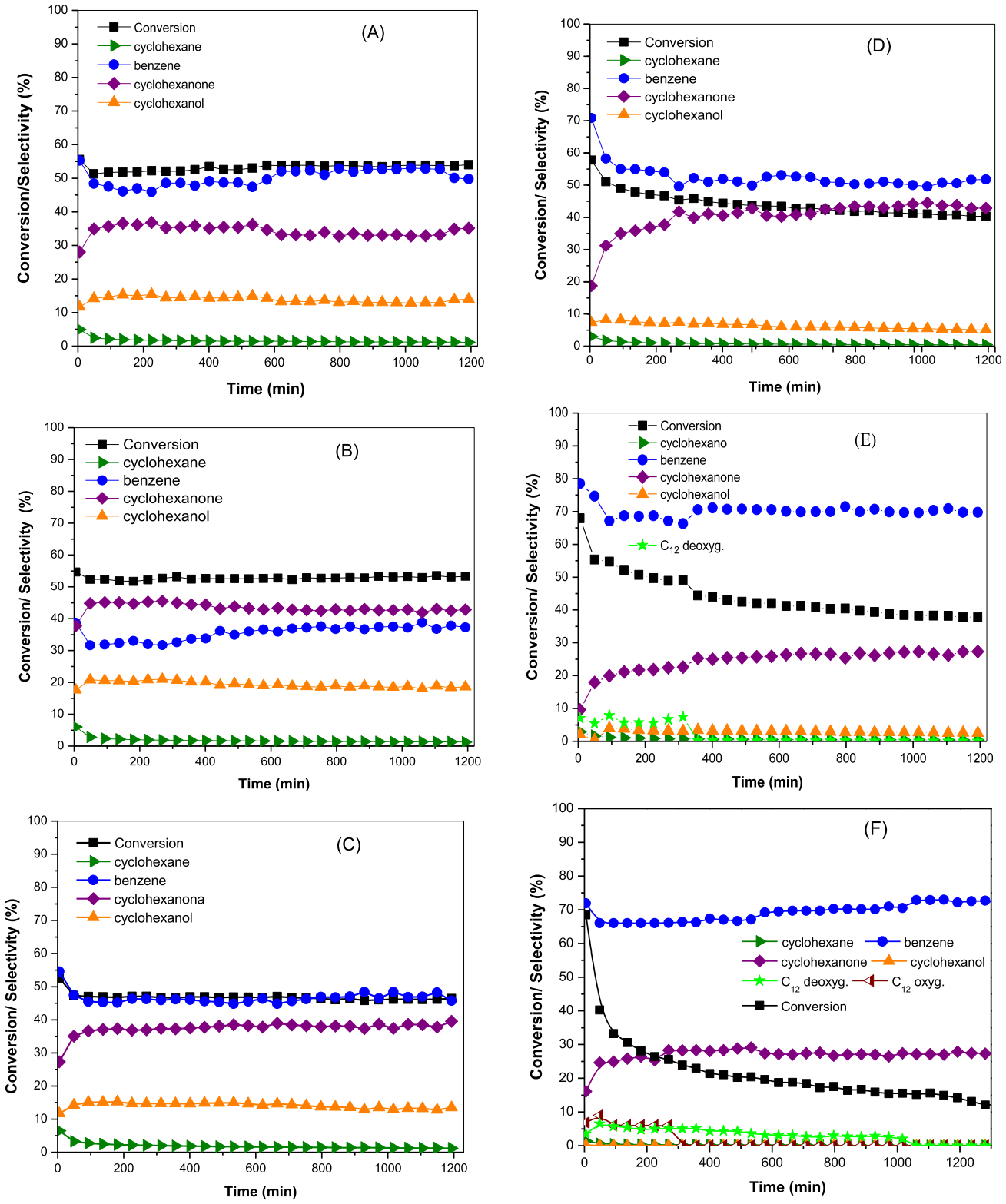

Fig. 8. Conversion of phenol and selectivity to products as a function of TOS for: (A) Pd/CeO_2; (B) $Pd/Ce_{0.75}Zr_{0.25}O_2$; (C) $Pd/Ce_{0.50}Zr_{0.50}O_2$; (D) $Pd/Ce_{0.25}Zr_{0.75}O_2$; (E) $Pd/Ce_{0.10}Zr_{0.90}O_2$; (F) Pd/ZrO_2.

metals, which did not produce benzene if supported on silica, showed significant formation of deoxygenated products in the presence of zirconia. This result reveals the important role of the support for the HDO of phenol. In fact, the deoxygenation activity takes place at the metal-support interface, with the activation of hydrogen occurring on the surface of metal particle.

For the case of acid-base oxide catalysts, the oxophilic sites are located at the exposed surface cations, which are expected to strongly bind oxygen and oxygenated groups. Recent calculations have shown that oxophilicity is directly correlated with the electronegativity of the cation [47].

The role played by the support (SiO_2, Al_2O_3, C and TiO_2) was also investigated by Newman et al. [17] for the HDO of phenol in liquid

phase over Ru supported catalysts. Titania supported Ru catalyst showed a notably higher benzene selectivity. In that case, following activation, Ti^{3+} sites interacted with oxygen from phenol, facilitating the cleavage of the C–O bond of phenol. de Souza et al. [15] investigated the effect of the type of support (SiO_2, Al_2O_3, TiO_2, ZrO_2, CeO_2 and $CeZrO_2$) on the performance of Pd-based catalysts for HDO of phenol at 573 K using a fixed bed reactor. The preference for benzene formation over Pd/TiO_2 and Pd/ZrO_2 was attributed to surface sites with greater oxophilicity due to incompletely coordinated Ti^{4+}/ Ti^{3+} and Zr^{4+}/Zr^{3+} cations located in close proximity to the periphery of metal particles. This enhanced interaction between support and oxygen in phenol increased the probability for hydrogenation of the C=O bond of the tautomer intermediate, resulting in a chemical promotion.

The strength of the interaction between the oxygen from the carbonyl group and the oxophilic site may be measured by DRIFTS of adsorbed cyclohexanone. Fig. 7c shows the fraction of the bands located in the medium/low wavenumber region and the selectivity to benzene as a function of Zr content. Both curves follow the same trend, indicating that higher the strength of the bond between oxygen from carbonyl and the oxophilic site, the higher the activity to deoxygenated products.

In fact, the oxophilicity of these catalysts is correlated to the structure of the $Ce_xZr_{1-x}O_2$ solid solution formed. Raman and XRD results revealed the presence of two different structures: cubic for the catalysts with x = 0.0 to 0.5 and tetragonal for x > 0.5. Each structure contains a different number of atoms at the surface. For instance, theoretical calculations showed that the tetragonal phase zirconia has a 4-fold higher number of atoms on the surface than cubic zirconia [48]. Therefore, the number of Zr^{4+}/Zr^{3+} cations exposed on the surface of $Ce_xZr_{1-x}O_2$ with tetragonal structure is significantly larger than that for cubic structure, which explains the higher oxophilicity of $Pd/Ce_xZr_{1-x}O_2$ catalysts with x > 0.5 (Fig. 7c). de Souza et al. [14] also observed an effect of zirconia structure on the activity and selectivity to deoxygenated products for HDO of phenol. The Pd/t-ZrO_2 catalyst exhibited the highest activity for HDO and selectivity to benzene, which was attributed to the higher accessibility of Zr cations to phenol molecules on the tetragonal structure.

3.4. Long-term catalytic experiments on $Pd/Ce_xZr_{1-x}O_2$ catalysts

The stability of the catalysts was compared at similar initial phenol conversion (around 60%) during 20 h of reaction. Fig. 8 shows the conversion of the phenol and product distribution as a function of time on stream (TOS) for all catalysts.

All catalysts deactivated during 20 h of TOS but the deactivation degree depended on the Ce/Zr molar ratio of the support. Pd/ZrO_2, $Pd/Ce_{0.10}Zr_{0.90}O_2$ and $Pd/Ce_{0.25}Zr_{0.75}O_2$ catalysts significantly deactivated during TOS, whereas the phenol conversion only slightly decreased for Pd/CeO_2, $Pd/Ce_{0.75}Zr_{0.25}O_2$ and $Pd/Ce_{0.50}Zr_{0.50}O_2$ catalysts. The stability of the catalysts defined by eq. (3) is listed in Table 7. Increasing the Zr content significantly decreased the stability of the catalysts.

Product distribution also depended on the Ce/Zr molar ratio. Benzene and cyclohexanone were formed over all catalysts. Cyclohexanol and small amounts of cyclohexane were also observed but their formation decreased as Zr content increased. For Pd/ZrO_2 and $Pd/Ce_{0.10}Zr_{0.90}O_2$ catalysts, C_{12} hydrocarbons were produced. Furthermore, product distribution varied with TOS. Benzene selectivity decreased and the formation of cyclohexanone increased as the phenol conversion decreased for all catalysts. In addition, the selectivity to cyclohexanol slightly increased at the beginning of the reaction, remaining constant with TOS. The selectivity to C_{12} hydrocarbons decreased with TOS.

In order to determine the nature of the surface species formed and follow their evolution during the HDO of phenol at 573 K on $Pd/Ce_xZr_{1-x}O_2$ catalysts, DRIFTS spectra were obtained during 6 h under reaction conditions and the results are shown in Figs. 9,10, S8, S9, S10 and S11 (supporting information).

Table 7
Stability factor calculated by eq. 3 for the catalysts.

Catalyst	Stability factor
Pd/CeO_2	0.96
$Pd/Ce_{0.75}Zr_{0.25}O_2$	0.96
$Pd/Ce_{0.50}Zr_{0.50}O_2$	0.84
$Pd/Ce_{0.25}Zr_{0.75}O_2$	0.60
$Pd/Ce_{0.10}Zr_{0.90}O_2$	0.40
Pd/ZrO_2	0.08

DRIFTS spectra under reaction conditions at 573 K over Pd/CeO_2 catalyst exhibited bands at 1169, 1265, 1485, 1589, 3013 and 3063 cm^{-1} (Fig. 9). These bands are assigned to the following vibrational modes of phenoxy species formed by dissociative adsorption of phenol: ν(CO) mono stretching mode (1265 cm^{-1}); ν (C = C_{ring}) of the aromatic ring (1485 and 1589 cm^{-1}); ν (C–H) stretching mode of the aromatic ring (3013 and 3063 cm^{-1}); and in-plane bending of OH group (1169 cm^{-1}). The intensity of these bands remained approximately constant and no additional bands were detected during the reaction.

$Pd/Ce_{0.75}Zr_{0.25}O_2$ exhibited the same bands observed for CeO_2 supported catalyst (Fig. S8). Furthermore, the spectra remained unchanged during 6 h of reaction. However, new bands were observed in the spectra of the $Pd/Ce_{0.50}Zr_{0.50}O_2$ catalyst (Fig. S9). Besides the bands characteristic of phenoxy species (1165, 1264, 1482, 1589, 3014 and 3063 cm^{-1}), bands appeared at 2933, 2854 as well as a shoulder at 1450 cm^{-1}, corresponding to the vibrational modes of adsorbed cyclohexanol. The intensity of these bands did not change during the reaction. For $Pd/Ce_{0.25}Zr_{0.75}O_2$ catalyst, bands characteristic of adsorbed phenoxy and cyclohexanol were noticed in the DRIFTS spectra (Fig. S10). However, the intensity of these bands slightly increased during the reaction. These changes were more important for $Pd/Ce_{0.10}Zr_{0.90}O_2$ (Fig. S11) and Pd/ZrO_2 (Fig. 10) catalysts. In these cases, the intensity of the bands increased 2 and 4-fold, respectively, during the reaction. Fig. 11 shows the variation in the intensity of these bands during reaction for all catalysts.

Comparing the results of long-term catalytic tests and the DRIFTS spectra, it is noticed the existence of a direct correlation between the phenol conversion and the intensity of all bands in the spectra. For $Pd/Ce_{0.10}Zr_{0.90}O_2$ and Pd/ZrO_2 catalysts, the phenol conversion significantly decreased (Fig. 8), whereas the intensities of the bands characteristic of adsorbed phenoxy and cyclohexanol increased as a function of TOS (Fig. 10). This result shows that deactivation is accompanied by an accumulation of intermediate species during the reaction. On the other hand, the phenol conversion only slightly decreased while the bands intensities remained relatively unchanged for Pd/CeO_2, $Pd/Ce_{0.75}Zr_{0.25}O_2$, and $Pd/Ce_{0.50}Zr_{0.50}O_2$ catalysts.

3.5. The role of reduced defects of the support on the stability of catalysts for HDO of phenol

Catalyst deactivation during HDO of phenol remains a critical issue for the development of efficient catalysts for this reaction. However, there are only few studies dedicated to investigating the causes of catalyst deactivation for the HDO reaction.

de Souza et al. [15] reported an important effect of the type of the support on catalyst deactivation. A strong deactivation was observed for Pd/SiO_2, Pd/Al_2O_3, Pd/TiO_2 and Pd/ZrO_2 catalysts, whereas Pd/CeO_2 only slightly deactivated during reaction. They proposed that the main cause for catalyst deactivation was Pd sintering and blocking of Lewis acid sites. The authors also suggested that the lower degree of deactivation of Pd/CeO_2 catalyst was likely due to the higher density of oxygen vacancies of these supports. However, they did not quantify the concentration of these oxygen vacancies.

For $Pd/Ce_xZr_{1-x}O_2$ catalysts, the degree of deactivation depended on the zirconia content. The highest degree of deactivation was observed

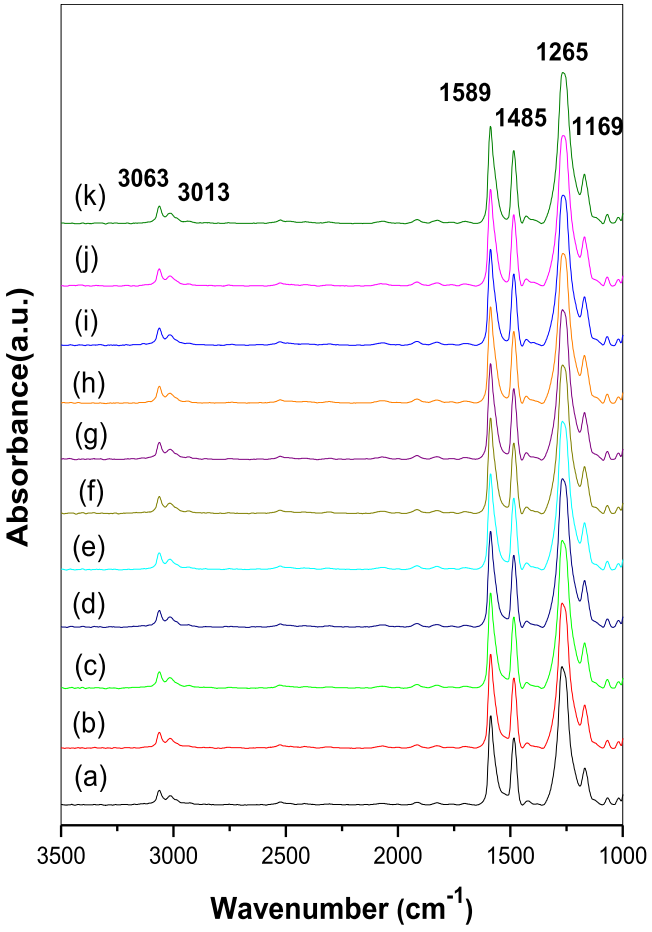

Fig. 9. DRIFTS spectra obtained over Pd/CeO_2 catalyst at 573 K and under the reaction mixture containing phenol + H_2 mixture during 6 h TOS: (a) 26; (b) 57; (c) 92; (d) 124; (e) 157; (f) 189; (g) 227; (h) 265; (i) 306; (*j*) 344; (k) 360 min.

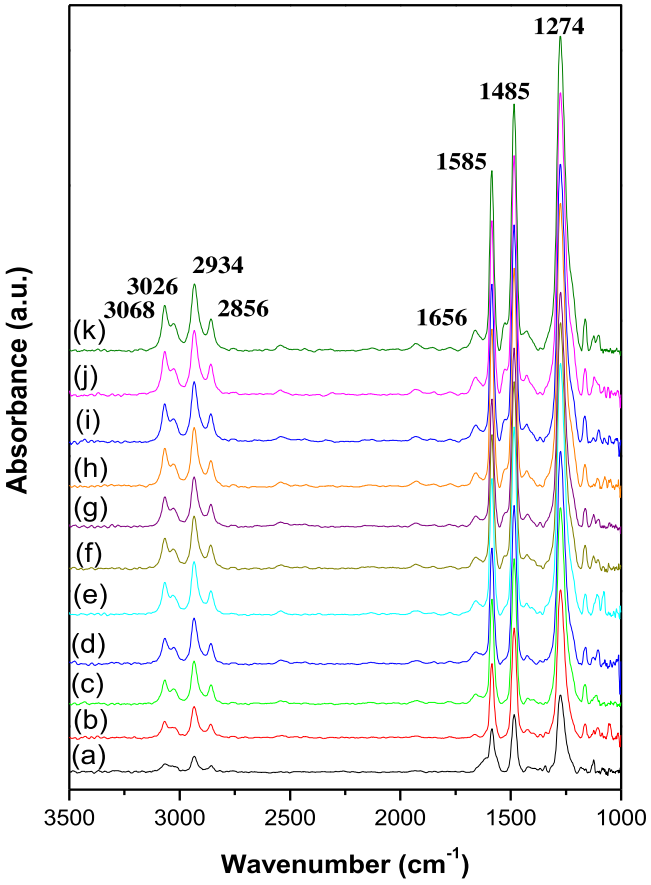

Fig. 10. DRIFTS spectra obtained over Pd/ZrO_2 catalyst at 573 K and under the reaction mixture containing phenol + H_2 mixture during 6 h TOS: (a) 34; (b) 60; (c) 87; (d) 112; (e) 151; (f) 198; (g) 231; (h) 268; (i) 309; (*j*) 349; (k) 358 min.

for Pd/ZrO_2, $Pd/Ce_{0.10}Zr_{0.90}O_2$ and $Pd/Ce_{0.25}Zr_{0.75}O_2$, whereas Pd/CeO_2, $Pd/Ce_{0.75}Zr_{0.25}O_2$ and $Pd/Ce_{0.50}Zr_{0.50}O_2$ catalysts were more stable and only slight losses in activity were detected. For Pd/ZrO_2 and Zr-rich catalysts, deactivation was accompanied by an accumulation of intermediate species during the reaction (Fig. 11). This result might be attributed to the loss of metal-support interface due to Pd sintering [15]. de Souza et al. [15] measured the variation of Pd dispersion during HDO reaction over Pd supported on different materials by the probe reaction of cyclohexane dehydrogenation reaction before and after 20 h of TOS. The ratio between the rate of cyclohexane dehydrogenation reaction before and after 20 h of TOS revealed that the growth of Pd particle during reaction, indicating that Pd sintering is one of the reasons for catalyst deactivation. This resulted in an accumulation of intermediate species, as shown by DRIFTS experiments under reaction conditions Curiously, Pd/CeO_2 catalyst remained quite stable during the reaction but showed a significant variation in Pd dispersion. This result could suggest that reduced defects play a role in the stability of this catalyst, removing carbon residues that were eventually formed. However, Raman spectroscopy of the spent catalysts was carried out and did not detect the presence of carbon residues on the surface of the catalysts. This result raises the question: Do reduced defects such as oxygen vacancies play a role in the stability of $Pd/Ce_xZr_{1-x}O_2$ catalysts for HDO of phenol?

In the present work, the reduced defect sites formed on the bulk and on the surface were determined by in situ XANES and XPS techniques.

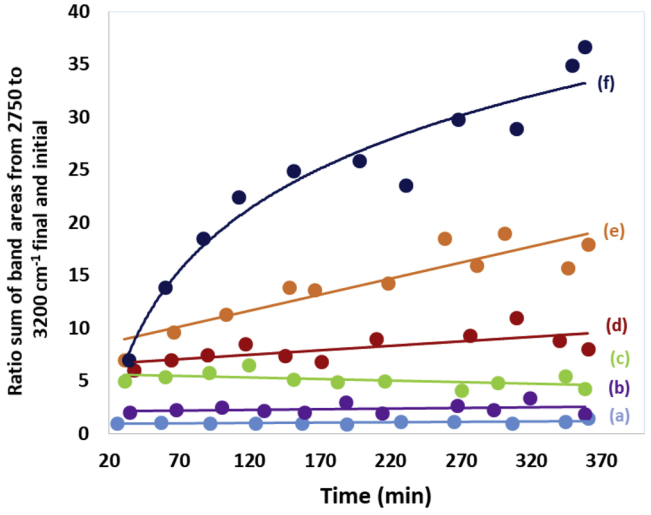

Fig. 11. Sum of band areas from 2750 to 3200 cm^{-1} in DRIFTS spectra obtained over (a) Pd/CeO_2; (b) $Pd/Ce_{0.75}Zr_{0.25}O_2$; (c) $Pd/Ce_{0.50}Zr_{0.50}O_2$; (d) $Pd/Ce_{0.25}Zr_{0.75}O_2$; (e) $Pd/Ce_{0.10}Zr_{0.90}O_2$; (f) Pd/ZrO_2.

The stability of the catalysts defined by eq. (3) was plotted as a function of the Zr content (Fig. 12). The stability remained constant up to x = 0.75 and then it significantly decreased. However, the fraction of Ce^{3+} species, determined by XANES (not shown) and XPS achieved a

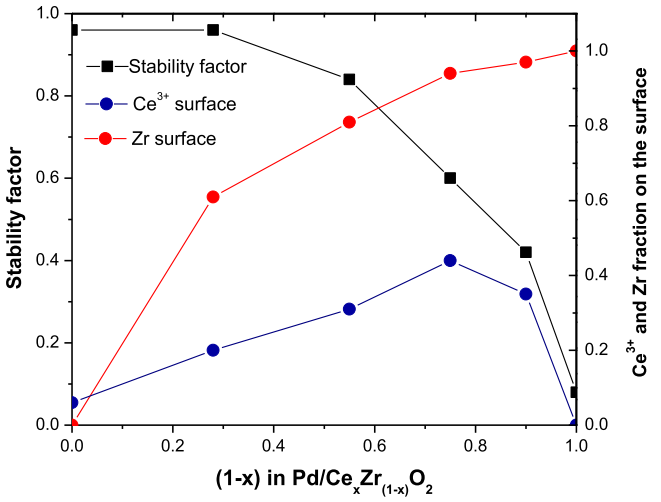

Fig. 12. The stability factor for HDO of phenol reaction and the fraction of Zr and Ce^{3+} species formed on the surface as a function of Zr content.

maximum at around 25% of Ce and then significantly decreased as the zirconia content increased. Therefore, it seems that there is no correlation between catalyst stability and the density of reduced defect sites formed on the support. In fact, the XANES experiments in the presence of water revealed that water dissociates on the oxygen vacancies to form bridging OH groups and ceria remains Ce^{3+}. Then, the oxygen vacancies might be occupied by the water formed on the reaction and they do not affect the stability of catalysts.

Fig. 12 also shows the fraction of Zr species formed on the surface as a function of Zr content. The fraction of Zr species on the surface increased as the zirconia loading increased. Comparing both curves, it is clear that the stability of the catalysts is related to the density of Zr species on the surface of the catalysts. The higher the fraction of Zr species on the surface the lower catalyst stability. The Raman and XRD techniques also showed the presence of a higher number of Zr cations on the $Ce_xZr_{1-x}O_2$ supports with tetragonal structure ($x > 0.50$), which contribute to the lower stability of these catalysts.

Furthermore, the DRIFTS of cyclohexanone also showed that the oxophilicity strongly depended on the Zr content. The oxophilicity increased as the zirconia loading increased. Thus, a stronger interaction between the oxygen of the tautomer intermediate and the Zr cation is expected for the Zr-rich catalysts. Therefore, the adsorption strength could contribute to catalyst deactivation by retaining more strongly adsorbed the intermediates formed, which agrees very well with the DRIFTS spectra. The stronger adsorption between the oxygen from the phenol with oxides such as ZrO_2 and $Ce_{0.10}Zr_{0.90}O_2$ resulted in an accumulation of O-containing byproducts and led to catalyst deactivation.

In fact, the main reaction pathway taking place on Pd/CeO_2, $Pd/Ce_{0.75}Zr_{0.25}O_2$ and $Pd/Ce_{0.50}Zr_{0.50}O_2$ catalysts is hydrogenation whereas the deoxygenation route occurs mainly on Pd/ZrO_2, $Pd/Ce_{0.10}Zr_{0.90}O_2$ and $Pd/Ce_{0.25}Zr_{0.75}O_2$. Therefore, the deoxygenation reaction is responsible for the deactivation. This can be seen plotting the TOF for the HDO reaction and the stability factor as a function of Zr content (Fig. 13).

4. Conclusions

This work studied the effect of the support properties on the performance of $Pd/Ce_xZr_{1-x}O_2$ catalysts with different compositions of Ce/Zr ($x = 0.00; 0.10; 0.25; 0.50; 0.75; 1.00$) for HDO of phenol in the gas phase at 573 K.

The activity and selectivity for hydrodeoxygenation of phenol depended significantly on the support composition. Comparing the behavior of selectivity to benzene with the values of the density of acid sites or the fraction of Ce^{3+} species on the surface and bulk as a function of Zr content, it is clear that there is no direct relationship between them. Rather, the activity and selectivity to deoxygenated products depend on the oxophilicity of the supports. The higher the strength between the carbonyl oxygen and oxophilic site (Zr^{4+}/Zr^{3+} cations), the higher the activity to deoxygenated products.

The degree of deactivation during the reaction depends on the Ce/Zr molar ratio of the support. Pd/ZrO_2, $Pd/Ce_{0.10}Zr_{0.90}O_2$ and $Pd/Ce_{0.25}Zr_{0.75}O_2$ catalysts readily deactivate during reaction, whereas Pd/CeO_2, $Pd/Ce_{0.75}Zr_{0.25}O_2$ and $Pd/Ce_{0.50}Zr_{0.50}O_2$ catalysts remains quite stable. The comparison between the results of long-term tests and DRIFTS spectra under reaction conditions revealed that deactivation is accompanied by an accumulation of intermediate species during the reaction. The strong adsorption strength (high deoxygenation activity) decreases the stability of the catalyst, due the accumulation of reaction intermediates that strongly interact with Zr cations in the support.

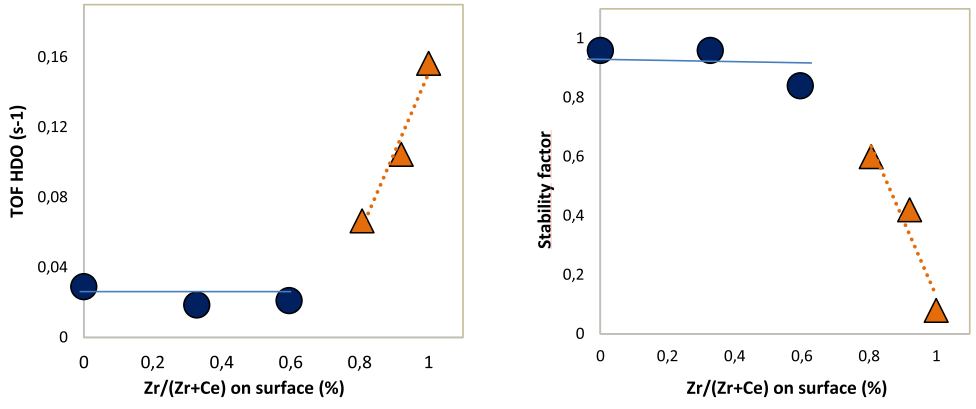

Fig. 13. (a) TOF to HDO reaction and (b) stability factor as a function of the content of Zr on surface. (circles) Pd/CeO_2; $Pd/Ce_{0.75}Zr_{0.25}O_2$; $Pd/Ce_{0.50}Zr_{0.50}O_2$; (triangles) $Pd/Ce_{0.25}Zr_{0.75}O_2$; $Pd/Ce_{0.10}Zr_{0.90}O_2$; Pd/ZrO_2.

Acknowledgments

The authors thank Conselho Nacional de Desenvolvimento Científico e Tecnológico (CNPq - 308200/2014-4), Coordenação de Aperfeiçoamento de Pessoal de Nível Superior (CAPES 001) and Fundação de Amparo à Pesquisa do Estado do Rio de Janeiro (FAPERJ) for the scholarship received and the financial support. Support from the National Science Foundation (EPSCoR0814361), US Department of Energy (DE-FG36GO88064), Oklahoma Secretary of Energy and the Oklahoma Bioenergy Center are greatly appreciated.

Appendix A. Supplementary data

Supplementary material related to this article can be found, in the online version, at doi:https://doi.org/10.1016/j.apcatb.2019.02.077.

References

[1] A. Demirbas, Appl. Energy 88 (2011) 17–28.
[2] T. Dickerson, J. Soria, Energies 6 (2013) 514–538.
[3] A. Foster, T.M.P. Do, R.F. Lobo, Top. Catal. 55 (2012) 118–128.
[4] H. Wan, R.V. Chaudhari, B. Subramaniam, Top. Catal. 55 (2012) 129–139.
[5] C.A. Teles, R.C. Rabelo-Neto, J.R. Lima, L.V. Mattos, D.E. Resasco, F.B. Noronha, Catal. Lett. 146 (2016) 1848–1857.
[6] Q. Tan, G. Wang, L. Nie, A. Dinse, C. Buda, J. Shabaker, D.E. Resasco, ACS Catal. 5 (2015) 6271–6283.
[7] M.B. Griffin, G.A. Ferguson, D.A. Ruddy, M.J. Biddy, G.T. Beckham, J.A. Schaidle, ACS Catal. 6 (2016) 2715–2727.
[8] L. Nie, P.M. de Souza, F.B. Noronha, W. An, T. Sooknoi, D.E. Resasco, J. Mol. Catal. A Chem. 388-389 (2014) 47–55.
[9] P.M. de Souza, R.C. Rabelo-Neto, L.E.P. Borges, G. Jacobs, B.H. Davis, T. Sooknoi, D.E. Resasco, F.B. Noronha, ACS Catal. 5 (2015) 1318–1329.
[10] C.A. Teles, R.C. Rabelo-Neto, G. Jacobs, B.H. Davis, D.E. Resasco, F.B. Noronha, ChemCatChem. 9 (2017) 2850–2863.
[11] A. Robinson, G.A. Ferguson, J.R. Gallagher, S. Cheah, G.T. Beckham, J.A. Schaidle, J.E. Hensley, J.W. Medlin, ACS Catal. 6 (2016) 4356–4368.
[12] I.T. Ghampson, C. Sepúlveda, A.B. Dongil, G. Pecchi, R. Garcia, J.L.G. Fierro, N. Escalona, Catal. Sci. Technol. 6 (2016) 7289–7306.
[13] A.J.R. Hensley, Y. Wang, J.-C. McEwen, ACS Catal. 5 (2015) 523–536.
[14] P.M. de Souza, R.C. Rabelo-Neto, L.E.P. Borges, G. Jacobs, B.H. Davis, U.M. Graham, D.E. Resasco, F.B. Noronha, ACS Catal. 5 (2015) 7385–7398.
[15] P.M. de Souza, R.C. Rabelo-Neto, L.E.P. Borges, G. Jacobs, B.H. Davis, D.E. Resasco, F.B. Noronha, ACS Catal. 7 (2017) 2058–2073.
[16] A.M. Barrios, C.A. Teles, P.M. de Souza, R.C. Rabelo-Neto, G. Jacobs, B.H. Davis, L.E.P. Borges, F.B. Noronha, Catal. Today 302 (2018) 115–124.
[17] C. Newman, X. Zhou, B. Goundie, I.T. Ghampson, R.A. Pollocck, Z. Ross, M.C. Wheeler, R. Meulenberg, R.N. Austin, B.G. Frederick, App. Catal. A: Gen. 477 (2014) 64–74.
[18] H.T. Chen, G. Pacchioni, ChemCatChem 8 (2016) 1–9.
[19] S.M. Schimming, O.D. LaMont, M. Konig, A.K. Rogers, A.D. D'Amico, M.M. Yung, C. Sievers, ChemChusChem 8 (2015) 2073–2083.
[20] W. Wang, K. Wu, P. Liu, L. Li, Y. Yang, Y. Wang, Ind. Eng. Chem. Res. 55 (28) (2016) 7598–7603.
[21] P.M. Mortensen, J.-D. Grunwaldt, P.A. Jensen, A.D. Jensen, ACS Catal. 3 (2013) 1774–1785.
[22] P. Pantu, G.R. Gavalas, App. Catal. A: Gen. 223 (2002) 253–260.
[23] R.J. Madon, M. Boudart, Ind. Eng. Chem. Fundam. 21 (1982) 438–447.
[24] C.E. Hori, H. Permana, K.Y. Ng Simon, A. Brenner, K. More, K.M. Rahmoeller, D. Belton, App. Catal. B: Environ. 16 (1998) 105–117.
[25] F.B. Passos, E.R. Oliveira, L.V. Mattos, F.B. Noronha, Catal. Today 101 (2005) 23–30.
[26] J.E. Spanier, R.D. Robinson, F. Zhang, S.-W. Chan, I.P. Herman, Phys. Rev. B 64 (2001) 245407–245408.
[27] R.C. Rabelo-Neto, M. Schmal App. Catal. A: Gen. 450 (2013) 131–142.
[28] P. Bouvier, H.C. Gupta, G.J. Lucazeau, J. Phys. Chem. Solids 62 (2001) 873–879.
[29] F.B. Noronha, E.C. Fendley, R.R. Soares, W.E. Alvarez, D.E. Resasco, Chem. Eng. J. 82 (2001) 21–31.
[30] A. Trovarelli, F. Zamar, J. Llorca, C. Leitenburg, G. Dolcetti, J.T. Kiss, J. Catal. 169 (1997) 490–502.
[31] A.I. Kozlov, D.H. Kim, A. Yezerets, P. Andersen, H.H. Kung, M.C. Kung, J. Catal. 209 (2002) 417–2426.
[32] J.C. Serrano-Luiz, J. Luettich, A. Sepúlveda-Escribano, F. Rodríguez-Reinoso, J. Catal. 241 (2006) 45–55.
[33] Silva AAA, A. A. A, N. Bion, F. Epron, S. Baraka, F.C. Fonseca, R.C. Rabelo-Neto, L.V. Mattos, F.B. Noronha, Effect of the type of ceria dopant on the performance of Ni/CeO_2 SOFC anode for ethanol internal reforming, App. Catal. B: Environ. 206 (2017) 626–641.
[34] A. Norman, V. Perrichon, A. Bensaddik, S. Lemaux, H. Bitter, D. Koningsberger, Topics Catal. 16 (2001) 363–368.
[35] M.C. Ribeiro, R.C. Rabelo-Neto, L.V. Mattos, G. Jacobs, B.H. Davis, F.B. Noronha, J. Phys. Chem. C 118 (2014) 28007–28016.
[36] F.L. Normand, L. Hilaire, K. Kili, G. Krill, G. Maire, J. Phys. Chem. 92 (1988) 2561–2568.
[37] D.R. Mullins, S.H. Overbury, D.R. Huntley, Surf. Sci. 409 (1998) 307–319.
[38] L. Qiu, F. Liu, L. Zhao, Y. Ma, J. Yao, App. Surf. Sci 252 (2006) 4931–4935.
[39] A. Corma, L.T. Nemeth, M. Renz, S. Valencia, Nature 412 (2001) 423–425.
[40] A. Corma, M.E. Domine, S. Valencia, J. Catal. 215 (2003) 294–304.
[41] T. Nimmawudipong, R.C. Runnebaum, K. Tay, D.E. Block, B.C. Gates, Catal. Lett. 141 (2011) 1072–1078.
[42] S.M. deLima, I.O. Cruz, G. Jacobs, B.H. Davis, L.V. Mattos, F.B. Noronha, J. Catal. 257 (2008) 356–368.
[43] R.C. Nelson, B. Baek, P. Ruiz, B. Goundie, A. Brooks, M.C. Wheeler, B.G. Frederick, L.C. Grabow, R.N. Austin, ACS Catal. 5 (2015) 6509–6523.
[44] J. Greeley, J.K. Nørskov, Surf. Sci. 592 (2005) 104–111.
[45] N. Duong, Q. Tan, C.R. Resasco, Chimie 21 (2018) 155–163.
[46] C.A. Teles, R.C. Rabelo-Neto, J.R. de Lima, L.V. Mattos, D.E. Resasco, F.B. Noronha, Catal. Letters 146 (2016) 1848–1857.
[47] K.P. Kappes, Inorg. Chem. 55 (2016) 9461–9470.
[48] G. Wang, F. Huang, X. Chen, S. Wen, C. Gong, H. Liu, F. Cheng, X. Zheng, G. Zheng, M. Pan, RSC Adv. 5 (2015) 85122–85127.